

---

# Generative Models of Visually Grounded Imagination

---

**Ramakrishna Vedantam**  
Virginia Tech  
vrama91@vt.edu

**Ian Fischer**  
Google Inc.  
iansf@google.com

**Jonathan Huang**  
Google Inc.  
jonathanhuang@google.com

**Kevin Murphy**  
Google Inc.  
kpmurphy@google.com

## Abstract

Consider how easy it is for people to imagine what a “purple hippo” would look like, even though they do not exist. If we instead said “purple hippo with wings”, they could just as easily create a different internal mental representation, to represent this more specific concept. To assess whether the person has correctly understood the concept, we can ask them to draw a few sketches, to illustrate their thoughts. We call the ability to map text descriptions of concepts to latent representations and then to images (or vice versa) *visually grounded semantic imagination*. We propose a latent variable model for images and attributes, based on variational auto-encoders, which can perform this task. Our method uses a novel training objective, and a novel product-of-experts inference network, which can handle partially specified (abstract) concepts in a principled and efficient way. We also propose a set of easy-to-compute evaluation metrics that capture our intuitive notions of what it means to have good imagination, namely correctness, coverage, and compositionality (the 3 C’s). Finally, we perform a detailed comparison (in terms of the 3 C’s) of our method with two existing joint image-attribute VAE methods (the JMVAE method of (Suzuki et al., 2017) and the bi-VCCA method of (Wang et al., 2016)) by applying them to two simple datasets based on MNIST, where it is easy to objectively evaluate performance in a controlled way.

## 1 Introduction

When we read or hear a word or phrase describing a concept, such as “A big bird”, it evokes, or conjures up, a mental picture in our head. This “picture” will be lacking many details — such as what kind of bird it is, what it is doing — but it will contain the “semantic essence”, or “intrinsic meaning”, of the concept. If we ask different people to generate images representing this concept, we expect to see some natural variation in the appearance, as they fill in details that were not specified in the text. This is because concepts are abstractions of the real world, that omit irrelevant details that are not central to the definition of the concept. However, we can always define more precise concepts by specifying extra features, such as “A big red bird”.

There are of course many kinds of concepts, and many ways to describe them. In this paper, we focus on visual concepts that correspond to single objects (as opposed to multi-object scenes), and we describe them using one or more attributes, which can be thought of as a simplified form of language. The advantage of attribute-based descriptions is that they are *compositional*, giving us an easy way to

specify novel concepts. For instance, we might never have seen any birds with the attributes “size”: small, “color”: white, but we can easily imagine such a concept.<sup>1</sup>

We can also use attributes to automatically create a subsumption (is-a) hierarchy or taxonomy: each node is a concept (a partial specification of certain attribute values), and its children are refinements of this concept, obtained by specifying the value of one or more “missing” attributes. Conversely, the parents of a node are abstractions of that node, obtained by unspecifying one or more attributes. For example, suppose the root of the tree corresponds to the abstract concept “bird”; the next level, which is slightly less abstract, contains the concepts “small birds”, “big birds”, “red birds”, “white birds”; below this we have “small white birds”, etc. The leaf nodes of the tree correspond to maximally specific, or concrete, concepts, where all attributes are specified. See Figure 1 for an illustration. We call this a *compositional concept hierarchy*. It differs from standard concept hierarchies, such as Wordnet (G. A. Miller, 1990) (which is the basis for Imagenet (Russakovsky et al., 2015)), in that it is algorithmically created by combining primitive attributes in all combinatorially possible ways. This is similar to the capacity of natural language to “make infinite use of finite means”, in the words of Noam Chomsky (1965).

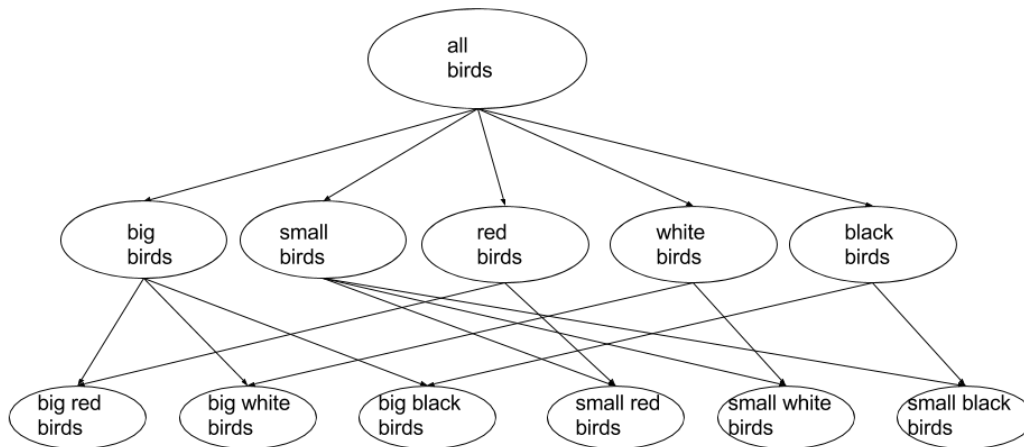


Figure 1: Illustration of a compositional concept hierarchy related to birds, derived from two independent attributes, size and color. Moving up the graph corresponds to abstraction of a concept; moving down the graph corresponds to refinement or specialization of a concept. The leaf nodes correspond to concrete, or maximally specific, concepts.

We would like to construct models that are able to “imagine” concepts from this concept hierarchy, given a linguistic description, and then “translate” this internal representation into an image. We call this ability *visually grounded semantic imagination*.

We argue that a good method for visually grounded semantic imagination should satisfy the following three criteria: (1) **Correctness**: The representation we create should match all the properties (attributes) that were mentioned (this is known as the *intension* of the concept). For example, if we say “red bird”, all the images we generate should contain birds that are red. (2) **Coverage**: The representation should only match the specified attributes, and should be indifferent to the values of the other unspecified attributes. This allows the representation to cover all of the different object variants that belong to that set (this is known as the *extension* of the concept). For example, if we say “red bird”, we should generate a diverse set of red birds — small ones, big ones, etc. (3) **Compositionality**: We should be able to imagine new concepts by adding or subtracting known building blocks (attributes). For example, if we have seen big red birds and small white birds, then we should be able to envision big white birds and small red birds; these correspond to concrete concepts that we have not seen before. We should also be able to envision abstract concepts, by generalizing from our concrete observations in different ways. For example, if we have seen big red birds and big

<sup>1</sup> If we have a class name, we can always include it as an extra ‘attribute’ if we wish. This will force some attributes to take on fixed values (e.g., if class=“robin”, then color=“red”, mammal=true), by definition of the class (cf., animals-with-attributes dataset (Lampert et al., 2013)); the remaining attributes are still free to vary, and can be thought of as optional adjectives modifying the noun (e.g., size can be big or small).

white birds, we should be able to imagine what big birds look like in general, learning to “factor out” the color of the bird. We call these criteria the *3 C’s of visual imagination*. We construct a setup, in terms of datasets and metrics, where each of these criteria can be measured in an objective way, as we explain in Section 2.

In Section 3, we show how we can extend the variational autoencoder (VAE) framework of (Kingma and Welling, 2014) to implement visually grounded semantic imagination. The first extension is to modify the model to the “multiple modality” setting<sup>2</sup>, where we have both an image,  $x$ , and an attribute vector,  $y$ . More precisely, we assume a joint generative model of the form  $p(x, y, z) = p(z)p(x|z)p(y|z)$ , where  $p(z)$  is the prior over latent variable  $z$ ,  $p(x|z)$  is our image decoder, and  $p(y|z)$  is our description decoder. We additionally assume that the description decoder factorizes over terms in the description, so  $p(y|z) = \prod_{k \in \mathcal{A}} p(y_k|z)$ , where  $\mathcal{A}$  is the set of possible attributes. (We can still model correlation between the attributes, if present, via the shared latent factors  $z$ .)

We further extend the Variational Autoencoder to devise a novel objective function, which we call the *triple ELBO*, for training the model. This fits three inference networks —  $q(z|x, y)$ ,  $q(z|x)$  and  $q(z|y)$  — so that at test time, we can embed an image or a description into the same shared latent space (using  $q(z|x)$  and  $q(z|y)$ , respectively); this lets us “translate” images into descriptions or vice versa, by computing  $p(y|x) = \int dz p(y|z)q(z|x)$  and  $p(x|y) = \int dz p(x|z)q(z|y)$ . Having the  $q(z|x)$  and  $q(z|y)$  inference networks, that can handle missing modalities, also lets us learn from images without descriptions, and descriptions without images, *i.e.*, we can perform semi-supervised learning.

Our third extension is a tractable way to handle partially specified concepts (*e.g.*, “big bird” does not specify the color). To do this, we introduce the notion of observed versus missing attributes. Let  $\mathcal{O} \subseteq \mathcal{A}$  represent the set of observed attributes, and  $y_{\mathcal{O}}$  their values. Since we assume attributes are conditionally independent, the corresponding likelihood is given by  $p(y_{\mathcal{O}}|z) = \prod_{k \in \mathcal{O}} p(y_k|z)$ . We also need to modify the inference network to handle missing inputs. Unlike the case of missing modalities, it is not feasible to fit a separate inference network for all  $2^{|\mathcal{A}|}$  possible missing attribute patterns. Instead, we use a method based on the product of experts (Hinton, 2002). In particular, our model has the form  $q(z|y_{\mathcal{O}}) \propto p(z) \prod_{k \in \mathcal{O}} q(z|y_k)$ . If no attributes are specified, the posterior is equal to the prior. As we condition on more attributes, the posterior becomes narrower, which corresponds to specifying a more precise concept. In Section 5, we show that this enables us to generate diverse images representing abstract concepts, as well as novel concrete concepts that were not seen during training.

In summary, the contributions of this paper are as follows. First, we define the notion of the 3C’s (consistency, coverage, and compositionality) for evaluating models of visually grounded imagination in an objective way. Second, we propose a novel loss function to train joint multi-modality VAEs, which we show outperforms previous approaches for grounded visual imagination. Third, we study how the use of attributes helps the model learn disentangled geometries in its latent space, which in turn supports the ability to perform abstraction and compositional generalization.

## 2 Evaluating visual semantic imagination

Visual imagination is the act of creating a latent representation of some concept. But how can we evaluate the quality these internal representations? Some papers (*e.g.*, (Chen et al., 2016; Higgins et al., 2017; Mathieu et al., 2016)) assess the quality of an internal representation by checking if it satisfies certain properties, such as being “disentangled”. A measure of disentanglement proposed for instance in Higgins et al. (2017) checks if the latent space captures the true factors of variation in simulated dataset, where we know the parameters of say a graphics engine, used for the simulation. However, we prefer to use an evaluation criterion that focuses on externally observable data, so that we can compare methods objectively using easily measured properties. We draw inspiration from the field of education, which similarly faces the challenge of assessing whether a student has successfully “understood” a concept (*c.f.*, (Piech et al., 2015)). With visual concepts, a natural approach is to give the student a description of the concept, and ask them to generate  $N$  images that match that description, by creating a set of images (*i.e.* the extension), which we denote by  $\mathcal{S}(y_{\mathcal{O}}) = \{x^{(n)} \sim p(x|y_{\mathcal{O}}) : n = 1 : N\}$ .

<sup>2</sup> We avoid the more common term “multi-modal”, since it may get confused with the notion of a probability distribution with multiple modes.

To evaluate the quality of these generated images, we apply a multi-label classifier to each one, to convert it to a predicted attribute vector,  $\hat{y}(x)$ . This classifier, which we call *observation classifier*, is trained beforehand on a large dataset of images and attributes, and is held constant across all methods that are being evaluated. It plays the role of a human observer. This is similar in spirit to generative adversarial networks (Goodfellow et al., 2014), that declare a generated image to be good enough if a binary classifier cannot distinguish it from a real image. (Both approaches avoid the problems mentioned in (Theis et al., 2016) related to evaluating generative image models in terms of their likelihood.) Given this classifier, we can measure the quality of the set of generated images using the 3 C’s, as we now discuss.

**Correctness.** We define correctness as the fraction of attributes for each generated image that match those specified in the concept’s description:

$$\text{correctness}(\mathcal{S}, y_{\mathcal{O}}) = \frac{1}{|\mathcal{S}|} \sum_{x \in \mathcal{S}} \frac{1}{|\mathcal{O}|} \sum_{k \in \mathcal{O}} \mathbb{I}(\hat{y}(x)_k = y_k). \quad (1)$$

We compute the correctness for the images generated given concrete (leaf node) as well as abstract concepts. We discuss how we create such concepts below.

**Coverage.** For coverage, we want to measure the diversity of values for the *unspecified* or missing attributes,  $\mathcal{M} = \mathcal{A} \setminus \mathcal{O}$ . One approach would be to compute the entropy of the distributions  $q_k$  for each  $k \in \mathcal{M}$ , where  $q_k$  is the empirical distribution over values for attribute  $k$  induced by set  $\mathcal{S}$ . However, since there may be correlation amongst the attributes (e.g., if most big birds are red), we instead compare  $q_k$  to  $p_k$ , which is the true distribution over values for attribute  $k$  for all images in the extension of  $y_{\mathcal{O}}$ . We can mix the true distribution with some prior in case there is poor coverage of the extension of some abstract  $y_{\mathcal{O}}$ , as might happen for more real datasets. We measure the difference between these distributions using the Jensen-Shannon divergence, since it is symmetric and satisfies  $0 \leq JS(p, q) \leq 1$ . We then define:

$$\text{coverage}(\mathcal{S}, y_{\mathcal{O}}) = \frac{1}{|\mathcal{M}|} \sum_{k \in \mathcal{M}} (1 - JS(p_k, q_k)). \quad (2)$$

We compute the coverage for a random sample of abstract (non-leaf) concepts, where at least one attribute is missing.

**Compositionality.** In standard supervised learning, we train on  $\mathcal{D}_{xy}^{\text{train}}$  and test on  $\mathcal{D}_{xy}^{\text{test}}$ , which are two disjoint labeled datasets of the form  $\{(x, y) \sim p_{\text{true}}(x, y)\}$ . We call this the iid setting. We usually assume that every class label in  $\mathcal{D}_{xy}^{\text{test}}$  has already been seen in  $\mathcal{D}_{xy}^{\text{train}}$ ; the iid setting therefore tests our ability to generalize across visual variation *within* known categories (attribute combinations).

To test our ability to generalize beyond the known categories, to novel combinations of attributes, we partition the label space  $Y$  into two disjoint subsets,  $Y_1$  and  $Y_2$ , such that for each  $y^{(2)} \in Y_2$ , there is no  $y^{(1)} \in Y_1$  that is identically equal, but there is some  $y^{(1)}$  which shares at least one attribute with  $y^{(2)}$ . For example, if  $Y = \{(b, r), (b, w), (s, r), (s, w)\}$ , represents the Cartesian product of (big, small) and (red, white), then a valid partition would be  $Y_1 = \{(b, r), (s, w)\}$  and  $Y_2 = \{(b, w), (s, r)\}$ .

Given this partition, let us define  $p_1(x, y) = p_{\text{true}}(x, y | y \in Y_1)$  as the distribution over images and concepts (descriptions) from split 1; define  $p_2(x, y) = p_{\text{true}}(x, y | y \in Y_2)$  similarly for split 2. We then create a training set from split 1,  $\mathcal{D}_{xy1}^{\text{train}} = \{(x, y) \sim p_1\}$ , train a model on it, and then evaluate it (in terms of correctness) on a test set from split 2,  $\mathcal{D}_{xy2}^{\text{test}} = \{(x, y) \sim p_2\}$ . A similar approach to studying compositionality was used in (Atzmon et al., 2016; Johnson et al., 2017; Agrawal et al., 2017). (This is also related to “zero shot learning”, as we discuss in the Section 4.)

In addition to measuring the ability to generalize to novel concrete concepts, we measure the ability to generalize to novel abstract concepts, where one or more attributes are not specified. (This is a different form of compositionality, in which we remove some parts of a concept’s definition, rather than rearranging existing parts.) For example, we might ask for the extension of big having trained with (big, red), and (big, white). Here the concept big has never been seen in isolation, and

in that sense the concept is novel for the model. We measure correctness and coverage of such abstract concepts. Note that this is identical to the experimental setup in coverage (2) above, we are just making the connection here that abstraction is also a form of compositional generalization.

### 3 VAE-based models for visual semantic imagination

We start by describing standard VAEs (Kingma and Welling, 2014), to introduce notation. We then discuss our extensions to handle the task of visually grounded semantic imagination.

**Standard VAEs.** A VAE (Kingma and Welling, 2014) is a latent variable model of the form  $p_\theta(x, z) = p_\theta(z)p_\theta(x|z)$ , where  $p(z)$  is the prior (we assume it is Gaussian,  $p(z) = \mathcal{N}(z|0, I)$ , although this assumption can be relaxed), and  $p(x|z)$  is the likelihood (sometimes called the decoder), usually represented by a neural network. To perform approximate posterior inference, we fit an inference network (sometimes called the encoder) of the form  $q_\phi(z|x)$ , so as to maximize the evidence lower bound or ELBO:

$$\text{elbo}(x) = E_{z \sim q_\phi(z|x)}[\log p_\theta(x|z)] - \text{KL}(q_\phi(z|x), p(z)) \quad (3)$$

where  $\text{KL}(p, q)$  is the Kullback Leibler divergence between distributions  $p$  and  $q$ . It is easy to show that  $\text{elbo}(x) \leq \log p(x)$ , so this is a form of approximate maximum likelihood training.

**Joint VAEs and the triple ELBO.** We extend the VAE to model images and attributes by defining the joint distribution  $p(x, y, z) = p(z)p(x|z) \prod_{k \in \mathcal{A}} p(y_k|z)$ , where  $p(x|z)$  is the image decoder (we use the DCGAN architecture from (Radford et al., 2015)), and  $p(y_k|z)$  is an MLP for the  $k$ 'th attribute, that maps  $z$  to a softmax distribution over the possible values for  $y_k$ . (For more details on the model architectures, see the supplementary material.)

If we only observe a single modality, we can marginalize out the non-observed variables. For example, if we just observe an image, and no attribute, the conditional likelihood becomes

$$\sum_y p(x, y|z) = \sum_y [p(x|z)p(y|z)] = p(x|z) \left[ \sum_y p(y|z) \right] = p(x|z) \quad (4)$$

Similarly, if we just observe a attribute, and no image, the conditional likelihood becomes  $p(y|z)$ .

In addition to the generative model, we fit an inference network of the form  $q(z|x, y)$ . To handle the case where we only have an image as input, we fit a  $q(z|x)$  network. Similarly, to handle the case where we only have a attributes as input, we also fit a  $q(z|y)$  network. So overall we fit three inference networks. The output of each of these networks is two vectors, one predicting the posterior mean of  $z$ , and one predicting its posterior covariance (we assume the covariance is diagonal for simplicity).

Our objective function for a single datapoint has the following form, which we call the *triple ELBO*:

$$\begin{aligned} \mathcal{L}(x, y) = & E_{q(z|x, y)}[\lambda_x^{xy} \log p(x|z) + \lambda_y^{yx} \log p(y|z)] - \text{KL}(q(z|x, y), p(z)) \\ & + E_{q(z|x)}[\lambda_x^x \log p(x|z)] - \text{KL}(q(z|x), p(z)) \\ & + E_{q(z|y)}[\lambda_y^y \log p(y|z)] - \text{KL}(q(z|y), p(z)) \end{aligned} \quad (5)$$

where  $\lambda_x^x, \lambda_y^y, \lambda_x^{xy}, \lambda_y^{yx}$  are scaling terms, chosen to balance the likelihood contribution of each type of data. (We discuss these terms in more detail later.)

**Justification for the triple ELBO.** We now give an intuitive justification for the triple ELBO objective. We want to ensure that the region of latent space occupied by each attribute vector  $y$  matches the region of latent space occupied by the set of corresponding  $(x, y)$  pairs, where  $x \in \mathcal{D}_{xy}$  is drawn from the set of images corresponding to  $y$ . More precisely, let  $q(z|\mathcal{D}_{xy}) = \frac{1}{|\mathcal{D}_{xy}|} \sum_{x \in \mathcal{D}_{xy}} q(z|x, y)$  be the ‘‘empirical posterior’’ for this grounding of the concept. We would like  $q(z|y)$  to match  $q(z|\mathcal{D}_{xy})$ , so it ‘‘covers’’ all the examples of the concept that it has seen. However, we don’t want to only put mass on the observed examples, or worse a single observed example, so we also want  $q(z|y)$  to be as entropic (*i.e.*, as close to the  $\mathcal{N}(0, I)$  prior) as possible. (The issue of how much to

generalize from a small set of examples of a concept, and along which feature dimensions, is also discussed in (Tenenbaum, 1999).)

As we explain in Section 4, different papers adopt different objectives for encouraging this behavior. In our approach, we rely on the triple ELBO. This encourages  $q(z|y)$  to be as close as possible to  $q(z|\mathcal{D}_{xy})$ , since the same decoder network  $p(y|z)$  is used for generating both the paired and unpaired data. Furthermore, the  $\text{KL}(q(z|y), p(z))$  term encourages  $q(z|y)$  to be as broad as possible, relative to the length scale defined by the prior.

However, we noticed empirically that sometimes the triple ELBO on its own is insufficient to enforce this desired behavior. To see why, consider generating an attribute vector  $y$ . If this attribute vector is paired with an image, the latent variable will be sampled from  $q(z|x, y)$ . If this is not paired with an image, it will be sampled from  $q(z|y)$ . We would like the model to use the same part of latent space in both cases, so that the representation is shared, but a powerful decoder could learn to map different parts of latent space to the same observation. To avoid this effect, we only train the parameters of the  $p(y|z)$  model in the  $\text{elbo}(x, y)$  term and not in the  $\text{elbo}(y)$  term. When optimizing the  $\text{elbo}(x, y)$  term on paired data, the model learns a latent representation based on aligned images and attributes. When optimizing the  $\text{elbo}(y)$  term, the model just needs to learn how to map into this precomputed embedding space. (In practice, we optimize all terms simultaneously, but conceptually it is helpful to think of a two-step process.) We call this variant of the model triple ELBO+FL, where FL stands for “frozen likelihood”.

**The role of the likelihood scaling terms.** If the image decoder  $p(x|z)$  is a Gaussian, then we can interpret  $\lambda_x^x \log p(x|z)$  as simply a rescaling of the precision of this Gaussian, since

$$\lambda_x^x \log p(x|z) = -\frac{\lambda_x^x}{2\sigma^2} (x - \mu(z))^T \Sigma(z)^{-1} (x - \mu(z))^2 + \text{const.}$$

where  $\mu(z)$  and  $\Sigma(z)$  are the outputs of the image decoder given input  $z$ . (Typically  $\Sigma(z)$  will be diagonal.)

When we have a uni-modality VAE, the scaled objective becomes

$$L = \lambda_x^x E_{q(z|x)} [\log p(x|z)] - \text{KL}(q(z|x), p(z)) \quad (6)$$

$$= E_{q(z|x)} [\log p(x|z)] - \beta_x \text{KL}(q(z|x), p(z)) \quad (7)$$

where  $\beta_x = 1/\lambda_x^x$ . This is equivalent to the  $\beta$ -VAE approach of (Higgins et al., 2017). They showed that by using  $\beta_x \gg 1$ , they could encourage the learning of a “disentangled” representation, since the posterior is forced to be closer to the  $\mathcal{N}(0, I)$  prior, which is already disentangled.

When we have a multi-modality VAE, the scaling terms affect not just how much we regularize towards the prior, but also how much each modality influences the latent space. When the modalities have different amounts of information, it is important to tune these scaling parameters appropriately. In particular, since an image is more informative than an attribute, we need to set  $\lambda_y^y > 1$ ,  $\lambda_x^x \leq 1$ , and  $\lambda_y^{yx}/\lambda_x^{xy} > 1$ ; this ensures that the latent space is shared between the attributes and the images, as we illustrate in Section 5.1.

**Product of Experts (PoE).** In order to handle missing attributes at test time, we assume that the  $q(z|y)$  inference network has the following form:  $q(z|y_{\mathcal{O}}) \propto p(z) \prod_{k \in \mathcal{O}} q(z|y_k)$ , where  $q(z|y_k) = \mathcal{N}(z|\mu_k(y_k), C_k(y_k))$  is the  $k$ ’th Gaussian “expert”, and  $p(z) = \mathcal{N}(z|\mu_0 = 0, C_0 = I)$  is the prior. This is similar to the product of experts model proposed in (Hinton, 2002), but differs in two ways. First, we include the “universal expert”  $p(z)$ , for reasons we discuss in Section 5.1. Second, we apply this model to represent the distribution of the latent variables, not the visible variables.

In (Hinton, 2002), each expert produced a distribution over binary variables, similar to a Boltzmann machine, and hence the normalization constant of the product was intractable. In our case, it can be shown that the (normalized!) product of all the Gaussian experts has the form  $q(z|y_{\mathcal{O}}) = \mathcal{N}(z|\mu, C)$ , where  $C^{-1} = \sum_k C_k^{-1}$  and  $\mu = C(\sum_k C_k^{-1} \mu_k)$ , where the sum is over all observed attributes plus the 0 term corresponding to  $p(z)$ . This equation has a simple intuitive interpretation: If we do not observe any attributes, the posterior reduces to the prior. As we observe more attributes, the posterior becomes narrower, since the (positive definite) precision matrices add up, reflecting the increased specificity of the concept being specified, as we show in Section 5.1.

Table 1: Summary of VAE variants.  $x$  represents some form of image, and  $y$  represents some form of annotation. For notational simplicity, we omit scaling factors for the ELBO terms. The objective in (Pandey and Dukkipati, 2017) cannot be expressed using our notation, since it does not correspond to a log likelihood of their model, even after rescaling.

Name	Ref	Model	Objective
VAE	(Kingma et al., 2014)	$p(z)p(x z)$	$\text{elbo}(x z; z x)$
triple ELBO	This	$p(z)p(x z)p(y z)$	$\text{elbo}(x, y z; z x, y)$ $+\text{elbo}(x z; z x) + \text{elbo}(y z; z y)$
JMVAE	(Suzuki et al., 2017)	$p(z)p(x z)p(y z)$	$\text{elbo}(x, y z; z x, y)$ $-\alpha\text{KL}(q(z x, y), q(z x))$ $-\alpha\text{KL}(q(z x, y), q(z y))$
bi-VCCA	(Wang et al., 2016)	$p(z)p(x z)p(y z)$	$\mu \text{elbo}(x, y z; z x)$ $+(1 - \mu)\text{elbo}(x, y z; z y)$
JVAE-Pu	(Pu et al., 2016)	$p(z)p(x z)p(y z)$	$\text{elbo}(x, y z; z x) + \text{elbo}(x z; z x)$
JVAE-Kingma	(Kingma et al., 2014)	$p(z)p(y)p(x z, y)$	$\text{elbo}(x y, z; z x, y) + \log p(y)$
CVAE-Yan	(Yan et al., 2016)	$p(z)p(x y, z)$	$\text{elbo}(x y, z; z x, y)$
CVAE-Sohn	(Sohn et al., 2015)	$p(z x)p(y x, z)$	$\text{elbo}(y x, z; z x, y; z x)$
CMMA	(Pandey et al., 2017)	$p(z y)p(x z)$	See text.

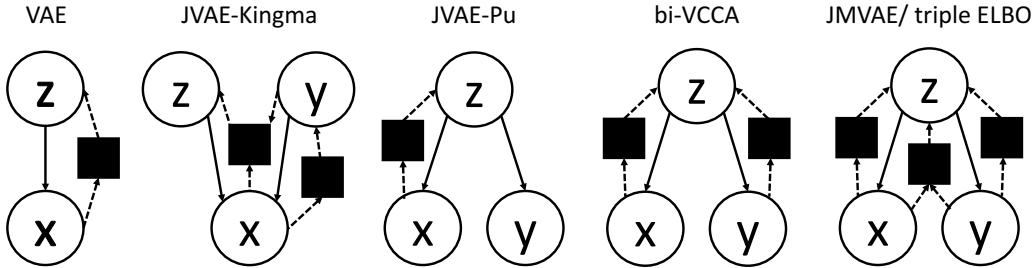


Figure 2: Summary of different (joint) VAEs. Circles are random variables, downward pointing arrows represent the generative (decoding) process, upward pointing arrows (with dotted lines) represent the inference (encoding) process, and black squares represent “inference factors”. Method names are defined in Table 1.

## 4 Related Work

The most closely related work is (Higgins et al., 2017), which came out 2 months after our paper was posted to arxiv. In their paper, they also fit a joint VAE to images and attribute vectors, but their objective function is slightly different. In particular, they replace the first term in our triple ELBO objective (Equation 5),  $E_{q(z|x,y)}[\log p(x, y|z)] - \text{KL}(q(z|x, y), p(z))$ , with  $\text{KL}(q(z|x), q(z|y))$ , thus avoiding the need to fit a  $q(z|x, y)$  inference network. (They still need aligned pairs from  $\mathcal{D}_{xy}$  for training, but they generate  $y$  by sampling from  $q(z|x)$  using an inference network  $q(z|x)$  which was “pretrained” in an unsupervised way on  $\mathcal{D}_x$ .) Their reverse KL term,  $\text{KL}(q(z|x), q(z|y))$ , encourages the  $q(z|y)$  posterior to “cover” the posterior induced by the corresponding images  $q(z|x)$ .

We do not need the reverse KL term, due to our need to generate aligned  $\mathcal{D}_{xy}$  data. In particular, we must use the same latent point  $z \sim q(z|x, y)$  when generating an image  $x$  and an attribute vector  $y$ ; let us denote the part of latent space that is sampled from (i.e., the support of  $q(z|x, y)$ ) by  $Z_{xy}$ . Now consider what happens when we fit the single modality datasets,  $\mathcal{D}_x$  and  $\mathcal{D}_y$ . When generating  $x$ , we sample from  $Z_x$ , and when generating  $y$ , we sample from  $Z_y$ . Since we use the same decoder in both the paired and unpaired settings, we find that  $Z_x \approx Z_y \approx Z_{xy}$ . Furthermore, the KL terms  $\text{KL}(q(z|y), p(z))$ ,  $\text{KL}(q(z|x), p(z))$  and  $\text{KL}(q(z|x, y), p(z))$  encourage the posteriors to be broad, so that  $Z_{xy}$  does not collapse to a single shared point.

(In addition to the above, rather technical, difference, (Higgins et al., 2017) consider learning logical combinations of two concepts, and learning mappings between different textual synonyms, which is something we cannot yet do with our model.)

In the sections below, we briefly summarize a variety of other papers that are also related, albeit not as closely as (Higgins et al., 2017).

**Conditional models.** Conditional VAEs (*e.g.*, (Yan et al., 2016; Pandey and Dukkipati, 2017)) and conditional GANs (*e.g.*, (Reed et al., 2016; Mansimov et al., 2016)) learn a stochastic mapping  $p(x|y)$  from semantics or attributes  $y$  to images  $x$ .<sup>3</sup> See Table 1 for a summary. Since these models treat  $x$  and  $y$  asymmetrically, they cannot compute both  $p(x|y)$  and  $p(y|x)$ , and do not support semi-supervised learning, unlike our joint method.

More importantly, these conditional models cannot handle missing inputs, so they cannot be used to generate abstract, partially specified concepts, such as “big bird”, as opposed to “big red bird”. One heuristic that is commonly used to adapt discriminative models so they can handle missing inputs is to set the unspecified input attributes, such as the bird’s color, to a special “UNK” value, and hope the network learns to “do the right thing”. Alternatively, if we have a joint model over inputs, we can estimate or impute the missing values when predicting the output image, as follows:

$$\hat{x}(y_{\mathcal{O}}) = \arg \max_y \log p(x|y) + \log p(y|y_{\mathcal{O}}) \quad (8)$$

(A similar approach was used in (Yan et al., 2016) to handle the case where some of the pixels being passed into an inference network  $q(z|x)$  were not observed.) However, conditioning on UNK or an imputed value is different than conditioning on nothing; only the latter will increase the posterior uncertainty in order to correctly represent less precise concepts with broader support.

**Joint VAEs.** Joint VAEs learn a joint probability distribution over  $x$  and  $y$ . (Wang et al., 2016; Pu et al., 2016; Suzuki et al., 2017) all use exactly the same generative model as us, namely  $p(x, y, z) = p(z)p(x|z)p(y|z)$ . The “semi supervised M2” model of (Kingma et al., 2014) uses a different joint model of the form  $p(x, y, z) = p(z)p(y)p(x|y, z)$ , which assumes that  $z$  captures aspects of the image (*e.g.*, style) that are not specified in  $y$  (*e.g.*, content). By contrast, our JVAE assumes that  $z$  captures all the aspects that are shared between  $x$  and  $y$ . The non-shared factors can be modeled implicitly by the stochasticity in the  $p(x|z)$  and  $p(y|z)$  decoders, or as additional explicit latent variables, as in “private VCCA” model of (Wang et al., 2016).

**Models for multiple modality data.** Various ways of learning representations from aligned  $(x, y)$  pairs have been proposed in the literature. The usefulness of such aligned cross-modality data for learning neural representations was pointed out in (de Sa and Ballard, 1998). It is also related to the infamous “symbol grounding problem” in philosophy (Harnard, 1990; Baroni, 2016).

Recently there has been a trend towards learning from *unaligned* multiple modality data (see *e.g.*, (Aytar et al., 2016)). However, this can cause problems when fitting VAEs. In particular, VAEs with powerful stochastic decoders (such as pixelCNNs for  $p(x|z)$  and RNNs for  $p(y|z)$ ), can excel at learning good single modality generative models, but may learn to ignore  $z$ , as pointed out in (Chen et al., 2017). This cannot happen with paired data, since the only way to explain the correlation between the two modalities is via the shared latent factors.<sup>4</sup>

**Training objectives for single modality inference networks.** In a JVAE, we may train on aligned data, but at test time, we usually only observe a single modality. Hence we must fit up to 3 inference networks,  $q(z|x, y)$ ,  $q(z|x)$  and  $q(z|y)$ . Several different objective functions have been proposed for this. To explain them all concisely, we define a modified version of the ELBO, where we distinguish between the variables we pass to the decoder,  $p(a|b)$ , the encoder,  $q(c|d)$ , and the prior,  $p(c|e)$ :

$$\text{elbo}(a|b; c|d; e) = E_{q(c|d)}[\log p(a|b)] - \text{KL}(q(c|d), p(c|e)). \quad (9)$$

If we omit the  $p(c|e)$  term, we assume we are using the unconditional  $p(c)$  prior. The objective functions used by various papers are shown in Table 1. In particular, the bi-VCCA objective of (Wang

<sup>3</sup> (Sohn et al., 2015) use a CVAE of the form  $p(y|x)$ , which corresponds to structured output prediction. In their examples,  $x$  is an image and  $y$  is a per-pixel labeling.

<sup>4</sup> If we do not have paired data, we could imagine duplicating the  $x$  signal and fitting a model of the form  $p(z)p(x|z)p(x|z)$ . However this would not encourage the model to learn meaningful structure in its latent space, since any unique hash of the image  $x$ , stored in the latent space, would be sufficient for good reconstructions, even though such a representation would have no generalization abilities. However, if we paired  $x$  with a noisy version of  $x$ , we could potentially learn a good latent representation, as in denoising autoencoders (Bengio et al., 2013). (The noisy MNIST experiments of (Wang et al., 2016) pair an image  $x$  of a digit with a noisy version of a different image, but which represents a digit with the same class label. However, this is not the same as using  $x$  and a noisy version of  $x$ , and in fact the only thing the two images have in common is the class label. So this technique relies on having (image, label) pairs.)

et al., 2016) has the form

$$\mu (E_{q(z|x)}[\log p(x, y|z)] - \text{KL}(q(z|x), p(z))) + (1-\mu) (E_{q(z|y)}[\log p(x, y|z)] - \text{KL}(q(z|y), p(z))) \quad (10)$$

and the JMVAE objective of (Suzuki et al., 2017) has the form

$$E_{q(z|x, y)}[\log p(x, y|z)] - \text{KL}(q(z|x, y), p(z)) - \alpha \text{KL}(q(z|x, y), q(z|y)) - \alpha \text{KL}(q(z|x, y), q(z|x)) \quad (11)$$

We see that the main difference between our approach and previous joint models is our use of the triple ELBO objective, which provides a different way to train the single modality inference networks  $q(z|x)$  and  $q(z|y)$ .

The problem with the bi-VCCA method of (Wang et al., 2016) is that the  $E_{q(z|y)} \log p(x, y|z)$  term causes the generation of blurry samples, and hence low correctness. The reason is that a single  $y$  is required to “explain” all the different  $x$ ’s to which it is matched, so it ends up being associated with their average. This problem can be partially compensated for by increasing  $\mu$ , but that reduces the  $\text{KL}(q(z|y), p(z))$  penalty, which is required to ensure  $q(z|y)$  is a broad distribution with good coverage of the concept.

A potential problem with the JMVAE method of (Suzuki et al., 2017) is that the addition of a penalty of the form  $\text{KL}(q(z|x, y), q(z|y))$  may result in lack of coverage of a concept, because  $q(z|y)$  should be a broad distribution, to cover all the variations of the concept, whereas  $q(z|x, y)$  will be close to a delta function, centered at the posterior mean  $\hat{z}(x, y)$ . (This is because there is usually little posterior uncertainty about the latent factors given an image.) However, in practice we find that JMVAE does about as well as our method. This is presumably because the  $\text{KL}(q(z|x, y), q(z|y))$  term is averaged over many  $(x, y)$  pairs, so  $q(z|y)$  will be close to  $q(z|\mathcal{D}_{xy})$  after all, as in our method.

The method of (Pu et al., 2016) is similar to ours, except it generates each  $(x, y)$  pair using  $z \sim q(z|x)$ , rather than  $z \sim q(z|x, y)$ . In practice, this is probably harmless, since  $y$  is often a deterministic function of  $x$  (since descriptions are abstractions of images). However, more problematic is that they do not fit a  $q(z|y)$  network, which is crucial for embedding semantics into the same latent space as images. Consequently we do not compare to their method.

**Gaussian embeddings.** There are many papers that embed images and text into points in a vector space. However, there are also a few that use Gaussian embeddings for words (Vilnis and McCallum, 2015; Athiwaratkun and Wilson, 2017), sometimes in conjunction with images (Mukherjee and Hospedales, 2016; Ren et al., 2016). Our method differs from these approaches in several ways.

First, we maximize the likelihood of  $(x, y)$  pairs, whereas the above methods learn a Gaussian embedding using a contrastive loss. In particular, they require data in which each word is paired with a “positive” word which appears in its context, and a “negative” word which does not. Although this is useful for learning distributional similarity, lexical context does not capture the kind of grounded semantics we are interested in (*e.g.*, it would hard distinguish the meanings of “left” and “right” using distributional semantics).

Second, our PoE formulation ensures that the covariance of the posterior  $q(z|y_{\mathcal{O}})$  is adaptive to the data that we condition on. In particular, it becomes narrower as we observe more attributes (because the precision matrices sum up), which is a property not shared by other embedding methods.

**Disentangled representations.** Several recent papers (*e.g.*, (Mathieu et al., 2016; Chen et al., 2016; Higgins et al., 2017; Denton and Birodkar, 2017) have explored ways to learn disentangled representations. The Beta-VAE method of (Higgins et al., 2017) is just like a regular VAE, except they use a coefficient of  $\beta \gg 1$  in front of the KL term, to encourage the posterior to be close to the (factorized) prior. (In our notation, this is equivalent to maximizing  $\text{elb}_{\text{O}_{1/\beta_x}}(x)$ .) The InfoGAN method of (Chen et al., 2016) partitions that latent space into an unstructured noise source  $z$  and an interpretable, factorized code  $c$ . They then fit a GAN with an additional term that tries to maximize the mutual information between  $c$  and the generated image,  $x = G(z, c)$ . In (Denton and Birodkar, 2017) two neural network encoders are forced to learn different aspects of video frames, content and pose. They use an adversarial discriminator to encourage this separation.

These methods have the advantage over ours in that they only need images and not attributes. However, it is not clear how to use these methods to learn more abstract forms of semantic structure in latent space (*e.g.*, consider representing the high-level concept “bird of prey” in a manner which

is orthogonal to its size and color), as our method is able to do (see Section 5). More generally, we argue that we need to have at least some labels or attributes in order to define what we mean by a good representation (Soatto and Chiuso, 2016). Effectively the labels define what we mean by “sufficient statistics”, but we can still use unlabeled data to learn the distribution of these statistics.

**Abstraction.** (Young et al., 2014) represent the extension of a concept (described by a noun phrase) in terms of a set of images whose captions match the phrase. By contrast, we use a parametric probability distribution in a latent space. (Vendrov et al., 2016) use order embeddings, where they explicitly learn subsumption-like relationships by learning a space that respects a partial order. In contrast, we reason about generality of concepts via the uncertainty induced by concepts in a visually grounded latent space.

**Visual imagination.** (Lin and Parikh, 2015) imagine abstract clipart scenes underlying text, and show improvements on the tasks of visual paraphrasing (determining if two sentences correspond to the same image) and fill-in-the-blanks. In a similar spirit, (Chen and Zitnick, 2015) predict CNN features at every step of an image caption generation model, thus imagining the grounding for words at every step. In contrast to these approaches, which use imagination as an intermediate step for solving downstream tasks, we are interested in probing the characteristics of good visual imagination (3 Cs) in a controlled setting, and we generate real images, not image features.

**Visual attributes.** There is a large literature on visual attributes (see *e.g.*, (Maji, 2017) for a good summary of recent papers). Perhaps the most relevant to our paper is (Misra et al., 2017), where they construct a compositional split of their (noun, adjective) data, and learn how to combine individual classifiers for nouns and adjectives to predict novel combinations (this is analogous to our approach in which we combine individual attribute experts). However, they do not use generative models, and do not consider abstraction or the 3 C’s.

**Zero-shot learning.** “Zero shot learning” (ZSL) corresponds to the task of training on examples from one set of categories,  $C_1$ , and testing on another set,  $C_2$  (see *e.g.*, (Xian et al., 2017) for a recent review). There is a close connection between ZSL, attributes and compositional splits. In particular, suppose we are provided with a known mapping from class labels to attributes,  $y = C2A(c)$ , and vice versa,  $c = A2C(y)$ . Let  $Y_1 = \{y = C2A(c) : c \in C_1\}$  be the attributes for classes in  $C_1$ ; define  $Y_2$  similarly.

We can now easily perform ZSL by learning an attribute classifier, as follows. First we train the classifier on images with attributes from  $Y_1$ , and then apply it to images with attributes from  $Y_2$ . Finally, we convert the predicted attribute vector into a class label. To do this, we need a way to handle the fact that the predicted attributes will typically be uncertain, and so taking the argmax for each dimension separately might not decode to a valid class name. However, we can decode at the word level using  $\hat{c}(x) = \arg \max_{c \in C} p(y = C2A(c)|x)$ . This works even if the class was not seen during training, as discussed in (Lampert et al., 2013).

In the notation of our paper, ZSL corresponds to training on  $\mathcal{D}_{xy1}^{\text{train}}$  and testing on  $\mathcal{D}_{xy2}^{\text{test}}$ . Alternatively, we could test on  $\mathcal{D}_{xy}^{\text{test}} = \mathcal{D}_{xy1}^{\text{test}} \cup \mathcal{D}_{xy2}^{\text{test}}$ ; this is known as “generalized ZSL” (Chao et al., 2016). This is harder than standard ZSL, although no explanation has been given to date, as far as we know. However, if we think of the problem in terms of decoding a probabilistic model, the reason becomes clear: conditioning on the fact that the attributes of the test examples are guaranteed to be in  $Y_2$  provides a constraint that can reduce the error rate, especially if  $Y_2$  is much smaller than  $Y_1$  (c.f., error correcting output codes (Dietterich and Bakiri, 1995)).

## 5 Experimental results

In this section, we compare various JVAE methods on two simple datasets derived from MNIST. We choose to use synthetic datasets so that we can control all the factors of variation explicitly; these can then be converted into a ground truth attribute set. This lets us easily evaluate methods in a rigorous, scientific way, which is often hard to do with “real world” datasets (cf., (Higgins et al., 2017), who use a synthetic dataset of 2d shapes, and (Johnson et al., 2017), who use a synthetic dataset of 3d shapes).

We first consider a very simple dataset that we fit with a JVAE with a 2d latent space, so that we can gain intuition into the various components of our method, and compare it to other methods. We then consider a slightly more complex dataset, and use it to perform a quantitative and qualitative comparison of our method with other methods in terms of the 3 C’s.

## 5.1 MNIST-2bit results

### 5.1.1 Dataset and Training.

In the first dataset, which we call “MNIST-2bit”, we modify MNIST by replacing the class id with two binary attributes which capture conceptual properties of the digit, namely its parity (whether it is odd or even), and its magnitude (whether it is small ( $< 5$ ) or big ( $\geq 5$ )). We fit the 2bit dataset using several VAE variants using a 2d latent space, to make visualization easy. We treat the pixels as binary and therefore use a Bernoulli likelihood for  $p(x|z)$ . For the attributes, we use a categorical likelihood for each  $p(y_k|z)$ .

All models in this section use triple ELBO without the fixed likelihood modification. Models were trained using Adam (Kingma and Ba, 2015) with a learning rate of 0.001 for 11,000 steps with a batch size of 64. Inspection of the loss curves indicated that the models converged easily on this task under these settings. For details on the model architecture, see the supplementary material.

### 5.1.2 Why we need annotations, and not just unlabeled images.

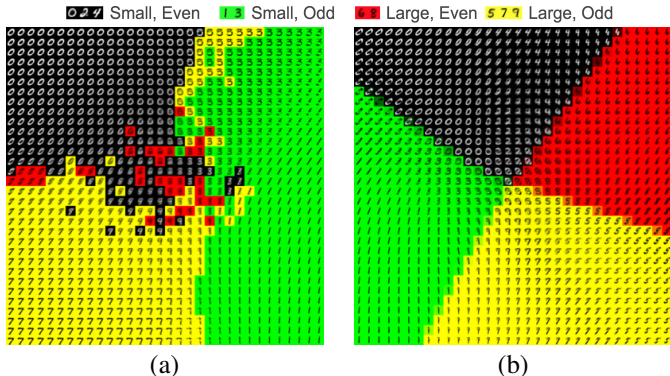


Figure 3: Visualization of the benefit of semantic annotations for learning a good latent space. Each small digit is a single sample generated from  $p(x|z)$  from the corresponding point  $z$  in latent space. (a)  $\beta$ -VAE fit to images without annotations. The color of a point  $z$  is inferred from looking at the attributes of the training image that maps to this point in space using  $q(z|x)$ . Note that the red region (corresponding to the concept of large and even digits) is almost non-existent. (b) Joint-VAE with  $\lambda_y^x = 50$  fit to images with annotations. The color of a point  $z$  is inferred from  $p(y|z)$ .

In Figure 3(a), we show the results of fitting a 2d  $\beta$ -VAE model (Higgins et al., 2017) to the images in MNIST-2bit, ignoring the attributes. We perform a hyperparameter sweep over  $\beta$ , and pick the one that gives the best looking latent space (this corresponds to a value of  $\beta = 10$ ). At each point  $z$  in the latent 2d space, we show a single image sampled from  $p(x|z)$ . To derive the colors for each point in latent space, we proceed as follows: we embed each training image  $x$  (with label  $y(x)$ ) into latent space, by computing  $\hat{z}(x) = E_{q(z|x)}[z]$ . We then associate label  $y(x)$  with this point in space. To derive the label for an arbitrary point  $z$ , we lookup the closest embedded training image (using  $\ell_2$  distance in  $z$  space), and use its corresponding label.

We see that the latent space is useful for autoencoding (since the generated images look good), but it does not capture the relevant semantic properties of parity and magnitude. In fact, we argue that there is no way of forcing the model to learn a latent space that captures such high level conceptual properties from images alone. (The same argument applies to any other way of learning “disentangled” latent spaces, such as InfoGAN (Chen et al., 2016).) A skeptic might complain that we have created an arbitrary partitioning of the data, that is unrelated to the appearance of the objects, and that learning such concepts is therefore “unnatural”. But consider an agent interacting with an environment by touching digits on a screen. Suppose the amount of reward they get depends on whether the digit that they touch is small or big, or odd or even. In such an environment, it would be very useful for

the agent to structure its internal representation to capture the concepts of magnitude and parity, rather than in terms of low level visual similarity. (In fact, (Scarf et al., 2011) showed that pigeons can learn simple numerical concepts, such as magnitude, by rewarding them for doing exactly this!) Language can be considered as the realization of such concepts, which enables agents to share useful information about their common environments more easily.

In Figure 3(b), we show the results of fitting a joint VAE model to MNIST-2bit, by optimizing  $\text{elbo}(x, y)$  on images and attributes (*i.e.*, we do not include the uni-modality  $\text{elbo}(x)$  and  $\text{elbo}(y)$  terms in this experiment.) Now the color codes are derived from  $p(y|z)$  rather than using nearest neighbor retrieval. We see that the latent space autoencodes well, and also captures the 4 relevant types of concepts. In particular, the regions are all convex and linearly separable, which facilitates the learning of a good imagination function  $q(z|y)$ , interpolation, retrieval, and other latent-space tasks.

### 5.1.3 Why we need the universal expert in the PoE inference network.

We now fit the generative model and three inference networks, using triple ELBO, so that we can visualize the posterior distribution over concepts using  $q(z|y)$ . In Figure 4(a), we visualize the  $2\sigma$  confidence ellipsoids derived from  $q(z|y)$ , where we use a non-PoE inference network. We see that for each of the 4 settings of  $y$ , there is an ellipse nicely contained inside the corresponding region of latent space. All the ellipses are axis aligned since we assume the covariance is diagonal.

In Figure 4(b), we show the results of fitting the same model, but this time using a PoE inference network, so we can compute the latent representation for abstract (partially specified) concepts. The 4 long and thin ellipses correspond to  $q(z|y_1 = 0)$ ,  $q(z|y_1 = 1)$ ,  $q(z|y_2 = 0)$ , and  $q(z|y_2 = 1)$ . We see that the model chooses to associate the horizontal axis (corresponding to latent subspace  $z_1$ ) to represent the magnitude attribute (large on the left, small on the right), and the vertical axis (corresponding to latent subspace  $z_2$ ) to the parity attribute (odd on the top, even on the bottom).

However, we also see that each individual Gaussian expert is rather long and thin. This can be problematic, since the elongation means that we are now in parts of the space which are unlikely w.r.t the prior, and thus can lead to sub-optimal samples. The reason this happens is the following: when all attributes are present (as is the case during training), the individual Gaussians get multiplied together, to produce a well defined results (as shown by the small ellipses in each quadrant), but at test time, when some attributes are missing, the product can be rather poorly behaved.

We can solve this problem by always including the universal expert  $p(z)$  in the product. The benefits of this are shown in Figure 4(c). We now get very nicely shaped posteriors for both concrete and abstract queries, since we always multiply each Gaussian expert, which may be long and thin, by the universal expert, which is a fixed sized circle.

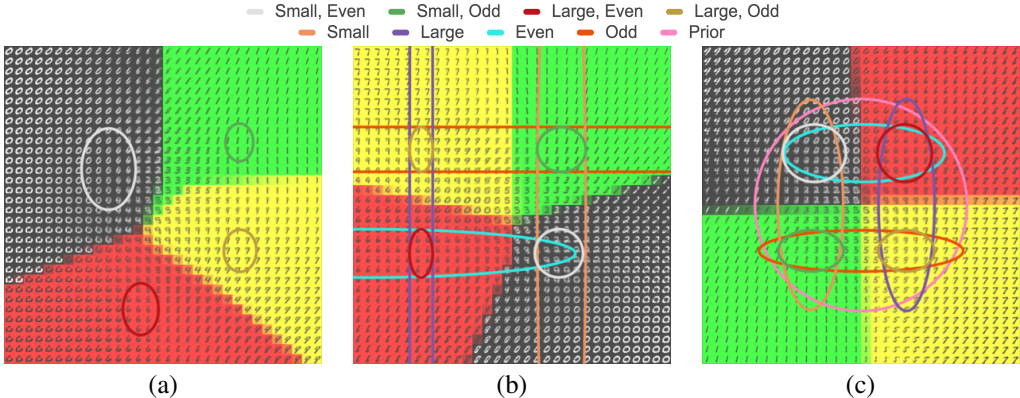


Figure 4: Visualization of the effect of using different inference networks. (For each experiment, we show the result obtained using the best hyperparameters.) (a) Product of Experts disabled,  $\lambda_x^x = \lambda_x^{xy} = 1$ ,  $\lambda_y^y = \lambda_y^{yx} = 10$ . (b) Product of Experts enabled, but no universal expert,  $\lambda_x^x = \lambda_x^{xy} = 1$ ,  $\lambda_y^y = \lambda_y^{yx} = 50$ . (c) Product of Experts enabled, with universal expert.  $\lambda_x^x = 0.001$ ,  $\lambda_x^{xy} = 0.1$ ,  $\lambda_y^y = \lambda_y^{yx} = 100$ . Figure best viewed by zooming in.

### 5.1.4 Why we need likelihood scaling terms.

In Figure 5(a), we show what happens if we optimize the unscaled triple ELBO objective. Without scaling the likelihood of  $y$ , the latent space is disorganized and imprecise with respect to the posteriors  $q(z|y)$  and the attributes predicted by  $p(y|z)$ . Note that in general, this does not imply poor classification or that the model does not know about the labels  $y$ , it merely means that a deep  $p(y|z)$  model can learn the appropriate invariances from the latent space to collapse them to the class label.

In Figure 5(b), we show the benefits of upweighting the likelihood of the labels. Now the latent space becomes well-organized and the posteriors align themselves nicely. However,  $p(x|z)$  and  $p(y|z)$  disagree on how to use the latent space, which results in the lower two regions having large numbers of incorrect digits (6s in the top left of the black region, and 0s in the bottom of the red region). This misalignment is due to  $q(z|x)$  not receiving any information about  $p(y|z)$ 's view of the latent space.

In Figure 5(c), we show the benefits of also downweighting the likelihood of the images, so that the  $p(x|z)$  term doesn't dominate when optimizing  $\text{elbo}(x)$ . Now the latent space becomes well-organized. By reducing the impact of  $p(x|q(z|x))$  on the loss for  $p(x|z)$ , the two generators can agree on the layout of the latent space, fully resolving misalignment issues.

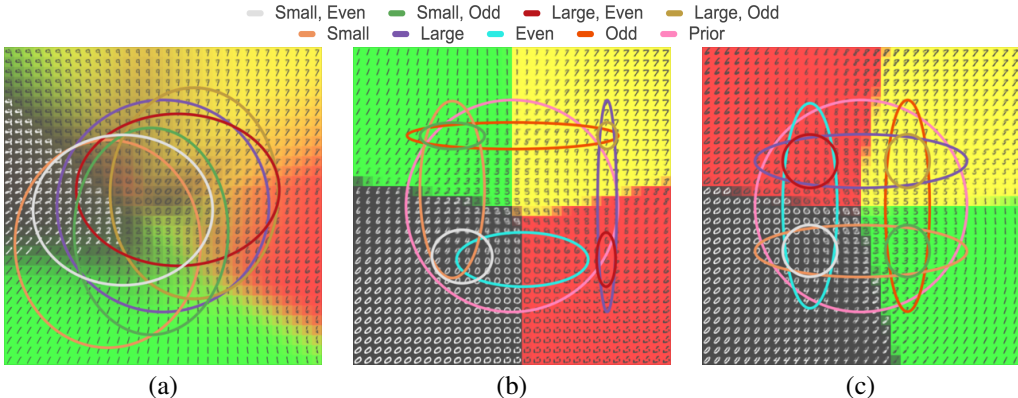


Figure 5: Visualization of the impact of likelihood scaling terms on the latent space. (a)  $\lambda_x^x = \lambda_x^{xy} = \lambda_y^y = \lambda_y^{yx} = 1$ . (b)  $\lambda_x^x = \lambda_x^{xy} = 1$ ,  $\lambda_y^y = \lambda_y^{yx} = 100$ . (c)  $\lambda_x^x = 0.01$ ,  $\lambda_x^{xy} = 1$ ,  $\lambda_y^y = \lambda_y^{yx} = 100$ . Figure best viewed by zooming in.

### 5.1.5 Understanding the Bi-VCCA objective.

Figure 6(a) shows the results of fitting the bi-VCCA model using  $\mu = 0.1$ . The model learns good axis-aligned attribute regions in  $z$  and corresponding good axis-aligned Gaussians with appropriate variance. However, these properties come at the expense of image reconstruction quality. All of the images are blurry, and many of them clearly combine two digits.

Figure 6(b) shows the results of fitting the bi-VCCA model using  $\mu = 0.9$ . Setting  $\mu$  to be large substantially improves image quality, but at the expense of  $p(y|z)$  producing less ideal regions. Even more problematic are the Gaussians generated by  $q(z|y)$ , which are all much too precise to give good generalization and coverage, as we will see below. In this case, the Gaussians for *small* and for *even* completely failed to appear in the shown region, which is a common occurrence for models that perform poorly at this task.

### 5.1.6 Understanding the JMVAE objective.

Figure 6(c) shows the results of fitting the JMVAE model using  $\alpha = 0.1$ . JMVAE consistently generates Gaussians with high variance. When  $\alpha$  is small, all of the Gaussians overlap heavily. In this case, the red Gaussian (*large, even*) is positioned over the black region (*small, even*) more fully than the white Gaussian, and vice-versa. The fact that  $p(x|z)$  and  $p(y|z)$  still perform well indicates that they are relying almost entirely on the signal from the  $q(z|x, y)$  network to solve the task.

Figure 6(d) shows the results of fitting the JMVAE model using  $\alpha = 10$ . When  $\alpha$  is large, the Gaussians correspond well to the attribute regions output by  $p(y|z)$ , meaning that larger values of

$\alpha$  lead to better alignment in our MNIST-2bit world. Note, however, that there is still more overlap between the concepts than when using triple ELBO (compare Figure 6(d) with Figure 5(c)).

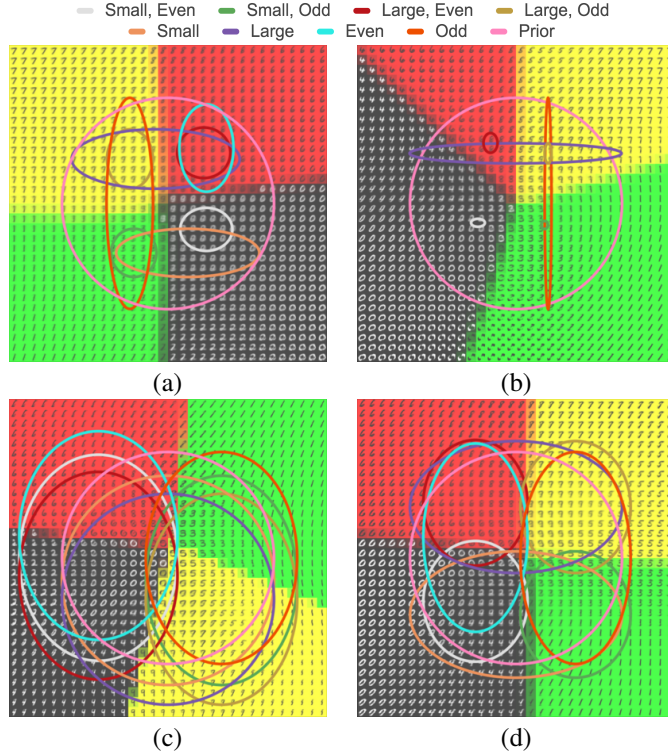


Figure 6: Effect of hyper-parameters on bi-VCCA and JMVAE. (a) bi-VCCA,  $\mu = 0.1$ . (b) bi-VCCA,  $\mu = 0.9$ . (c) JMVAE,  $\alpha = 0.1$ . (d) JMVAE,  $\alpha = 10$ . Figure best viewed by zooming in.

## 5.2 MNIST-a Results

### 5.2.1 Dataset.

In this section, we use a slightly more complex dataset which we call “MNIST-a”, which stands for “MNIST with attributes”. This is created by modifying the original MNIST digits as follows. We first create a compositional concept hierarchy using 4 discrete attributes, corresponding to class label (10 values), location (4 values), orientation (3 values), and scale (2 values) (note that the two values we use for scale (big, small) refer to the visual size of the digit, whereas in Section 5.1, scale referred to the numerical magnitude). Thus there are  $10 \times 2 \times 3 \times 4 = 240$  unique concepts in total.

Next we create  $\sim 2916$  example images of each concept by sampling real-valued transformation parameters from truncated Gaussian distributions associated with each attribute value, and then applying the corresponding affine transformation to randomly chosen MNIST digits of the corresponding class.<sup>5</sup> We call this the `iid` dataset. We split this into a train, validation and test set using 85%, 5% and 10% of the data, respectively.

We also create a compositional split of the data (denoted `comp`), where we put 85% of the concepts (204) in the training set, 5% of the concepts (12) in the validation set, and 10% of the concepts (24) in the test set. The splits are chosen so that each attribute vector only appears in one of the three sets. We convert the training concepts into a dataset of images and attributes by extracting images with matching attributes from the `iid` dataset.

<sup>5</sup> More precisely, we generated the dataset as follows: for each of the 70k original MNIST images, we sampled 10 attribute vectors uniformly at random (keeping the class label consistent with the chosen image); we then generated 10 versions of the original image, resulting in a dataset of 700k labeled images. Thus each concept has about  $700,000/240 \approx 2916$  images associated with it. Note that the transformed images are grayscale, just like the original MNIST dataset. We binarize the images for training and evaluation. See the supplementary material for details.

In addition to the 240 concrete concepts, we create a set of abstract concepts as follows: for each level of abstraction (obtained by dropping 1, 2, or 3 of the attributes), we make 2 variants of each of the 240 possible concepts by dropping different attributes at random, resulting in 480 abstract concepts per level. We repeat the above process of random dropping independently for train, val and test splits giving us three sets of abstract queries. (Note that we do not use the abstract training set, since we only train on concrete concepts; but we do use the abstract validation and test concepts for evaluating model performance.)

### 5.2.2 Evaluation methodology.

We compare various models on both the `iid` and `comp` datasets. We then evaluate performance in terms of correctness and coverage of concrete and abstract concepts. More precisely, we consider the following scenarios: (1) train on `iid`, evaluate correctness on previously seen concrete concepts; (2) train on `iid`, evaluate correctness and coverage on abstract concepts; (3) train on `comp`, evaluate correctness on novel concrete concepts. We do not evaluate coverage of concrete concepts, since even a single sample will suffice to cover a concept in which all attributes are specified (providing all the attributes for the sample match all the attributes of the concept, *i.e.*, the sample is correct).

To measure correctness and coverage, we need to convert a sampled image into an attribute vector. For this, we train the observation classifier on the full `iid` dataset, where it gets to an accuracy of 91.18% for class label, 90.56% for scale, 92.23% for orientation, and 100% for location. Consequently, it is a reliable way to assess the quality of samples from various generative models.

### 5.2.3 Models and training.

For the image models,  $p(x|z)$  and  $q(z|x)$ , we use the DCGAN architecture from (Radford et al., 2015)). For the attribute models,  $p(y_k|z)$ ,  $q(z|y_k)$  and  $q(z|y_{1..K})$ , we use MLPs. For the joint inference network,  $q(z|x, y)$ , we use a CNN combined with an MLP. We use  $d = 10$  latent dimensions for all models. See supplementary material for details.

We train each model using three objectives: triple ELBO, JMVAE and bi-VCCA. We use Adam (Kingma and Ba, 2015) for optimization, with a learning rate of 0.0001, and a minibatch size of 64. We train all models for 500,000 steps (we generally found that the models do not tend to overfit in our experiments).

### 5.2.4 Hyper-parameters.

For each model, we have to choose various hyperparameters: the label likelihood weighting  $\lambda_y^{yx} \in \{1, 10, 50\}$  (we keep  $\lambda_x^{xy} = 1$  fixed throughout), and whether to use PoE or not for  $q(z|y)$ . In addition, each way of training the model has its own method-specific hyperparameters: for JMVAE, we choose  $\alpha \in \{0.01, 0.1, 1.0\}$  (the same set of values used in (Suzuki et al., 2017)); for bi-VCCA, we choose  $\mu \in \{0.3, 0.5, 0.7\}$ ; for triple ELBO, we choose  $\lambda_y^y \in \{1, 50, 100\}$  (we keep  $\lambda_x^x = \lambda_x^{xy} = 1$ ). Thus all methods have the same number of hyperparameters.<sup>6</sup> We choose hyperparameter values based on performance on the relevant validation set. See the supplementary material for more details.

For triple ELBO, we find that it is critical to make  $\lambda_y^y$  sufficiently large; for example, if we set  $\lambda_y^y = 1$ , the correctness score of triple ELBO on concrete concepts drops from 90.67% to 53.43%. This is consistent with the results in Section 5.1, which showed the importance of upweighting the likelihood of the attributes relative to the images.

In terms of the  $q(z|y)$  model, we found that requiring it to be a PoE model (with universal expert), as opposed to an unrestricted inference network, slightly reduced performance, from 90.67% to 87.34% (for the triple ELBO model). Therefore, in the following experiments, we only report PoE numbers when evaluating abstract concepts.

<sup>6</sup> For triple ELBO, an additional decision is whether to use the fixed likelihood (which only updates  $p(y|z)$  in the  $\text{elbo}(x, y)$  term) or not. We found that turning it off dropped the correctness score from 90.67% to 85.78%. This is because learning the latent space using labels alone will not result in good alignment to images. We therefore keep FL turned on throughout the remaining experiments.

Table 2: Comparison of different approaches on MNIST-a test set. Higher numbers are better. Error bars (in parentheses) are standard error of the mean. For concrete concepts (where all 4 attributes are specified), we do not use a PoE inference network, and we do not report coverage. Hyperparameter settings for each result are discussed in the supplementary material.

Method	#Attributes	Coverage (%)	Correctness (%)	PoE?	Training set
triple ELBO	4	-	<b>90.76 (0.11)</b>	N	iid
JMVAE	4	-	86.38 (0.14)	N	iid
bi-VCCA	4	-	80.57 (0.26)	N	iid
triple ELBO	3	<b>90.76 (0.21)</b>	77.79 (0.30)	Y	iid
JMVAE	3	89.99 (0.20)	<b>79.30 (0.26)</b>	Y	iid
bi-VCCA	3	85.60 (0.34)	75.52 (0.43)	Y	iid
triple ELBO	2	<b>90.58 (0.17)</b>	<b>80.10 (0.47)</b>	Y	iid
JMVAE	2	89.55 (0.30)	77.32 (0.44)	Y	iid
bi-VCCA	2	85.75 (0.32)	75.98 (0.78)	Y	iid
triple ELBO	1	<b>91.55 (0.05)</b>	<b>81.90 (0.48)</b>	Y	iid
JMVAE	1	89.50 (0.09)	81.06 (0.23)	Y	iid
bi-VCCA	1	87.77 (0.10)	76.33 (0.67)	Y	iid
triple ELBO	4	-	<b>83.10 (0.07)</b>	N	comp
JMVAE	4	-	79.34 (0.52)	N	comp
bi-VCCA	4	-	75.18 (0.51)	N	comp

### 5.2.5 Evaluating correctness.

We start by evaluating the quality of models in terms of how correct their samples are. More precisely, for models trained on the iid dataset, we consider each of the 240 concrete concepts, and generate 10 images from each. For each generated image, we evaluate how many of the attributes were correctly predicted, and then compute the average correctness for that concept, and then average over concepts.

The results are shown in Table 2. Focusing on the concrete iid concepts (first block of the table), we see that triple ELBO (90.76%) outperforms JMVAE (86.38%), and both methods do significantly better than bi-VCCA (80.57%). To gain more insight, Figure 7 shows 4 samples from each of these 3 methods for 2 different concrete concepts, one chosen at random (bottom row), and one chosen where the discrepancy in correctness between triple ELBO and bi-VCCA was maximal.

We see that the images generated by bi-VCCA are much blurrier than the other methods, and are considered incorrect by the observation classifier. The blurriness is because of the  $E_{q(z|y)}[\log p(x, y|z)]$  term, as we discussed above. For all of our experiments, we use a value of  $\mu = 0.7$ , which reduces blurriness, and yields the best correctness score on the validation set. Nevertheless, this does not completely eliminate blurriness, as we can see.

From Figure 7 we see that the JMVAE samples look good. However, it sometimes makes mistakes by generating fragments of digit where there should not be any. This is illustrated in the bottom row, bottom left JMVAE sample, where there is some “ghosting” when generating the digit 1. This may be because there is no  $\text{KL}(q(z|y), p(y))$  term, which encourages the posterior to be close to the prior, reducing the chance of the model sampling a  $z$  vector far from the “familiar” part of latent space.

Table 2 also shows that the correctness scores for all methods are lower on abstract concepts than for concrete concepts. For example, triple ELBO drops from 90.76% to 77.79% when we move from conditioning on 4 attributes to 3. There are two reasons for this. First, when evaluating abstract concepts, we have to use the PoE inference network, which is somewhat less accurate than models that do not make the PoE assumption. Second, abstract concepts are effectively novel concepts that have never been seen before (since the model is trained only on concrete concepts). Indeed, we see that the correctness on abstract concepts is comparable to the correctness on concrete, but compositionally novel, concepts, as shown in the last block of the table. (We discuss the compositional results in more detail below.)

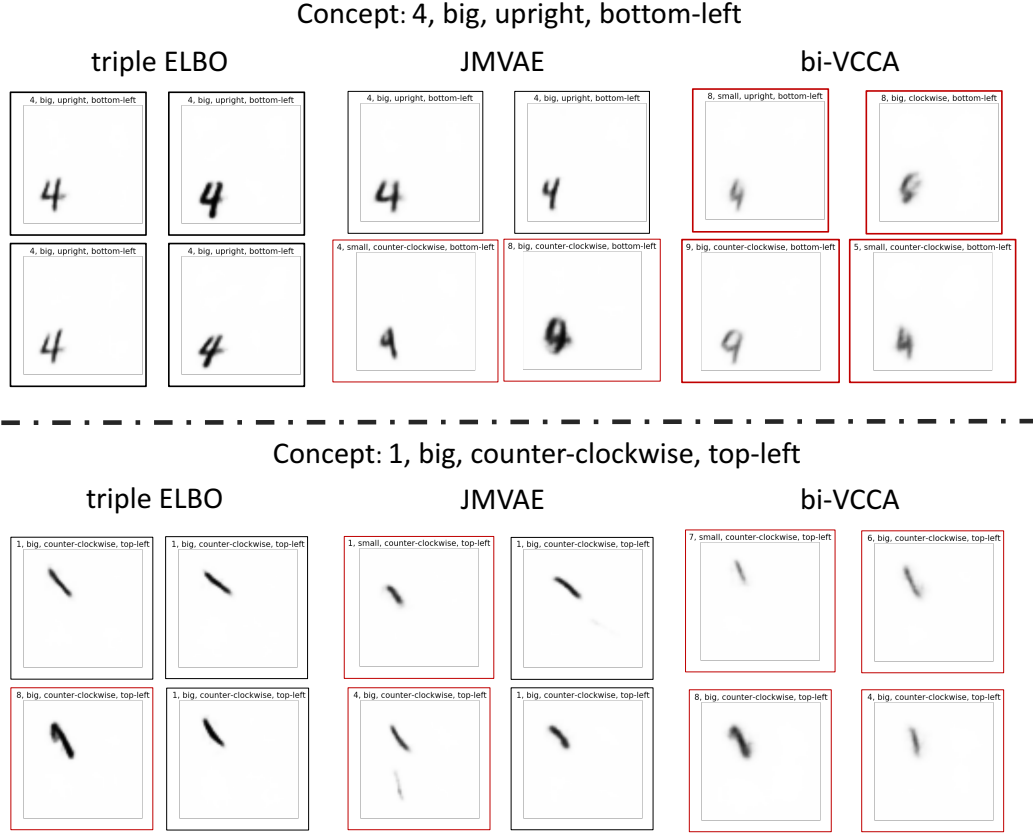


Figure 7: Samples of 2 (previously seen) concrete concepts using 3 different models. For each concept, we draw 4 samples from the posterior,  $z_i \sim q(z|y)$ , convert each one to a mean image,  $\mu_i = E[x|z_i]$ , and then show the results. The caption at the top of each image (in small font) is the predicted attribute values. (The observation classifier is fed sampled images, not the mean image that we are showing here.) The border of the image is black if all attributes are correct, otherwise the border is red.

### 5.2.6 Evaluating coverage.

In this section, we evaluate how well each method covers a concept, in terms of the diversity of the samples it generates. Note that we only apply this to abstract concepts, since concrete concepts fully specify all attributes, and hence a single sample automatically covers the entire concept.

The results are shown in Table 2. Once again, we see that triple ELBO outperforms JMVAE (although the gap is small), and both methods outperform bi-VCCA. To get a better understanding of how well the methods work, Figure 8 shows some sampled images for concepts at different levels of abstraction. In general we see that the samples are correct (consistent with the attributes that were specified), yet relatively diverse, as desired. (Note, however, that we manually selected 6 from 10 samples to make the figure. Automatically generating a diverse set of samples is left to future work.)

### 5.2.7 Evaluating compositionality.

In this section, we evaluate how well methods handle compositionally novel, concrete concepts. The results are shown in Table 2. We see that the correctness scores are lower for all methods than for concrete concepts in the iid setting. This is not surprising, since we are asking the model to extrapolate rather than interpolate.

As before, we see that triple ELBO outperforms JMVAE which outperforms bi-VCCA. To gain some insight, Figure 9 shows some images sampled by the 3 different methods in response to 2 compositionally novel concrete concepts. We see that bi-VCCA seems to have mostly generated 8's, no matter what the true concept. The samples from JMVAE in the top row look reasonable, but in the

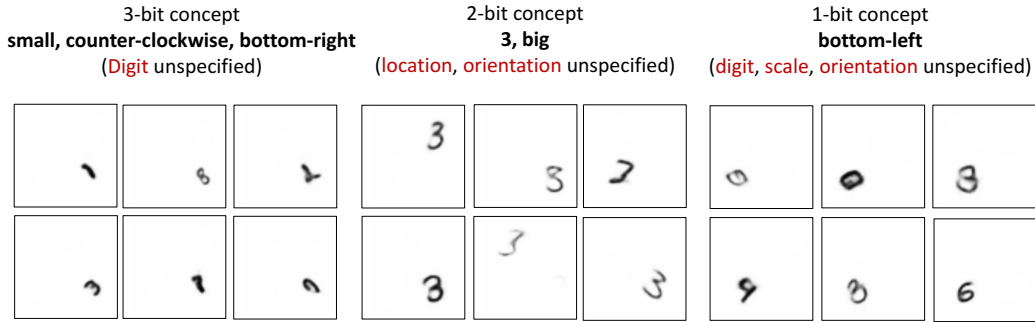


Figure 8: Samples of 3 abstract concepts using the triple ELBO model. More precisely, for each concept, we draw 10 samples from the posterior,  $z_i \sim q(z|y)$ , convert each one to a mean image,  $\mu_i = E[x|z_i]$ , and then manually pick the 6 most diverse ones to show here.

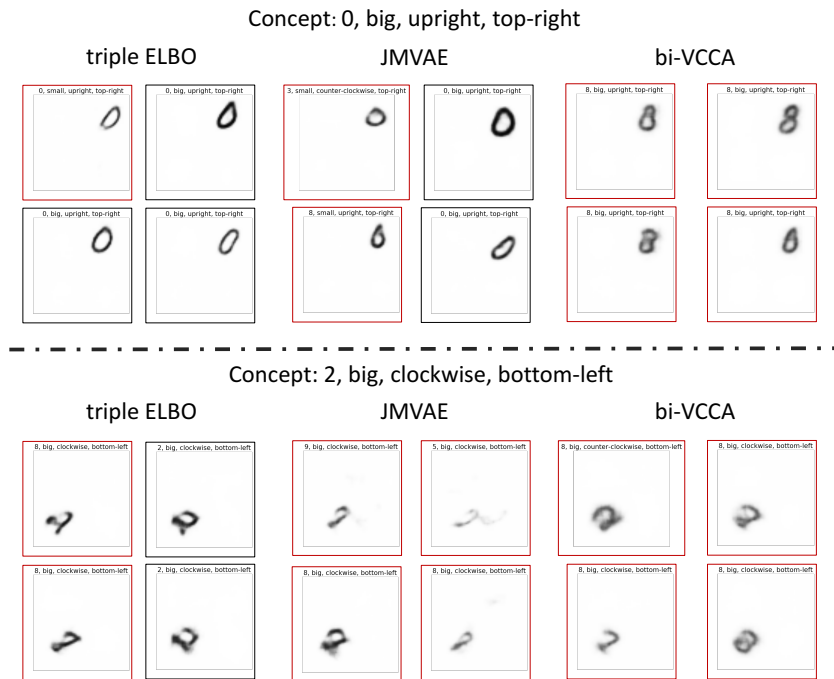


Figure 9: Samples of 2 compositionally novel concrete concepts using 3 different models. For each concept, we draw 4 samples from the posterior,  $z_i \sim q(z|y)$ , convert each one to a mean image,  $\mu_i = E[x|z_i]$ , and then show the results. The color coding is the same as Figure 7, namely red border means one or more attributes are incorrect (according to the observation classifier), black border means all attributes are correct.

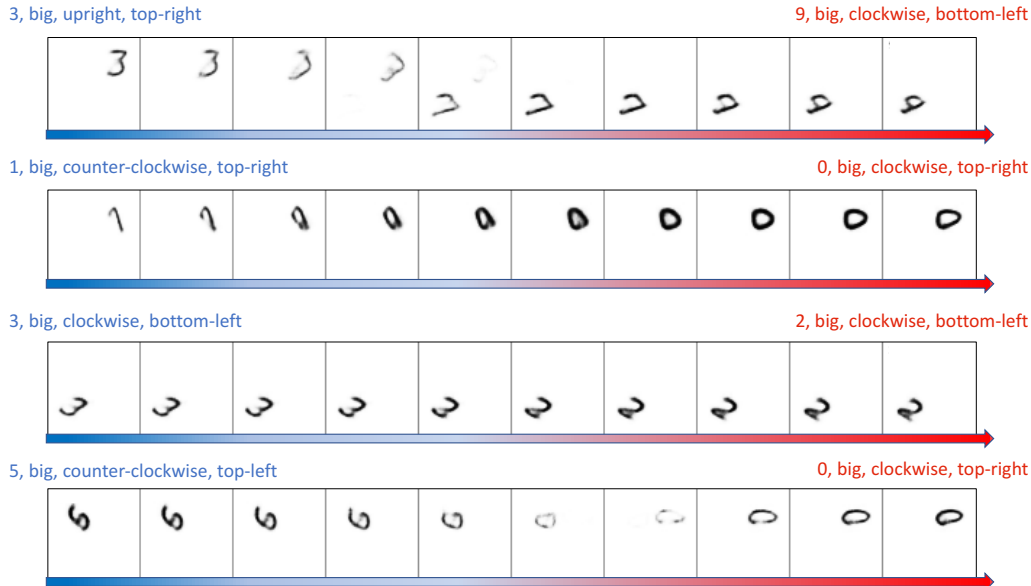
bottom row, they are of very poor quality, with a lot of ghosting; these artefacts are correctly detected by the observation classifier.

### 5.2.8 Semantic interpolation with compositionally novel concepts.

The inference network  $q(z|y)$  lets us imagine concepts specified by previously unseen descriptions  $y$ , as we discussed in Section 5.2.7. But we can also imagine novel concepts at a finer level of granularity than obtainable by changing discrete attributes, by moving through the continuous latent space. Following (White, 2016), we perform spherical interpolation between two “anchor” points,  $z_1$  and  $z_2$ . However, instead of computing these anchors by embedding two *images*,  $x_1$  and  $x_2$ , we can compute these anchors by embedding two *descriptions*,  $y_1$  and  $y_2$ , which lets us interpolate between concepts we have never seen before. More precisely, we sample anchors from the posterior,  $z_1 \sim q(z|y_1)$ , and  $z_2 \sim q(z|y_2)$ , and then perform spherical interpolation to create a path of points

$z_i$ . For each point in latent space, we compute the mean image  $\mu_i = E_{p(x|z_i)}[x]$ . We show example results in Figure 10. The model is able to generate plausible hallucinations of novel concepts purely from symbolic descriptions.

Figure 10: Results of interpolating in latent space between compositionally novel concepts. Each row contains two concrete concepts, on the left and right side; we then spherically interpolate between these two concepts in latent space, visualize the resulting mean image generated in pixel space. These results use the triple ELBO model trained on the comp dataset using the optimal hyperparameters (PoE off, fixed likelihood on,  $\lambda_y^y = 10$ ,  $\lambda_x^x = 1$ ,  $\lambda_x^{xy} = 1$ ,  $\lambda_y^{yx} = 10$ ,  $d = 10$  latent dimensions).



## 6 Conclusions and future work

We have shown how we can learn to represent the semantic content of images and descriptions using probability distributions over random vectors in a shared latent space. We use this to “imagine” compositionally novel concrete and abstract concepts, which we then “ground” into images, which we can evaluate in a simple, objective way.

In the future we would like to explore richer forms of description, beyond attribute vectors, such as natural language text. This will require replacing the  $p(y|z)$  and  $q(z|y)$  models with something more powerful, such as an RNN. We would also like to apply the technique to real world images, and to extend it to other tasks, such as image retrieval.

## 7 Supplementary Material

### 7.1 Details on the MNIST-a dataset

We created the MNIST-a dataset as follows. Given an image in the original MNIST dataset, we first sample a discrete scale label (big vs. small), an orientation label (clockwise, upright, and anti-clockwise), and a location label (top-left, top-right, bottom-left, bottom-right).

Next, we converted this vector of discrete attributes into a vector of continuous transformation parameters, using the procedure described below. We then the following steps. We first take an empty black canvas of size 64x64, rotate the original 28x28 MNIST image, and then scale and translate the image and paste it on the canvas. (We use bicubic interpolation for scaling and resizing the images.) Finally, we use the method of (Salakhutdinov and Murray, 2008) to binarize the images. See Figure 11 for example images generated in this way.

We convert the discrete attributes into a continuous transformation as follows:

- **Scale:** For big, we sample scale values from a Gaussian centered at 0.9 with a standard deviation of 0.1, while for small we sample from a Gaussian centered at 0.6 with a standard deviation of 0.1. In all cases, we reject and draw a sample again if we get values outside the range  $[0.4, 1.0]$ , to avoid artifacts from upsampling or problems with illegible (small) digits.
- **Orientation:** For the clockwise label, we sample the amount of rotation to apply for a digit from a Gaussian centered at  $+45$  degrees, with a standard deviation of 10 degrees. For anti-clockwise, we use a Gaussian at  $-45$  degrees, with a standard deviation of 10 degrees. For upright, we set the rotation to be 0 degrees always.
- **Location:** For location, we place Gaussians at the centers of the four quadrants in the image, and then apply an offset of  $\text{image\_size}/16$  to shift the centers a bit towards the corresponding corners. We then use a standard deviation of  $\text{image\_size}/16$  and sample locations for centers of the digits. We reject and draw the sample again if we find that the location for the center would place the extremities of the digit outside of the canvas.

We repeat the above process of sampling labels, and applying corresponding transformations, to generate images 10 times for each image in the original MNIST dataset. Each trial samples labels from a uniform categorical distribution over the sample space for the corresponding attribute. Thus, we get a new MNIST-a dataset with 700,000 images from the original MNIST dataset of 70,000 images. We split the images into a train, val and test set of 85%, 5%, and 10% of the data respectively to create the IID split. To create the compositional split, we split the  $10 \times 2 \times 3 \times 4 = 240$  possible label combinations by the sample train/val/test split, giving us splits of the dataset with non-overlapping label combinations.

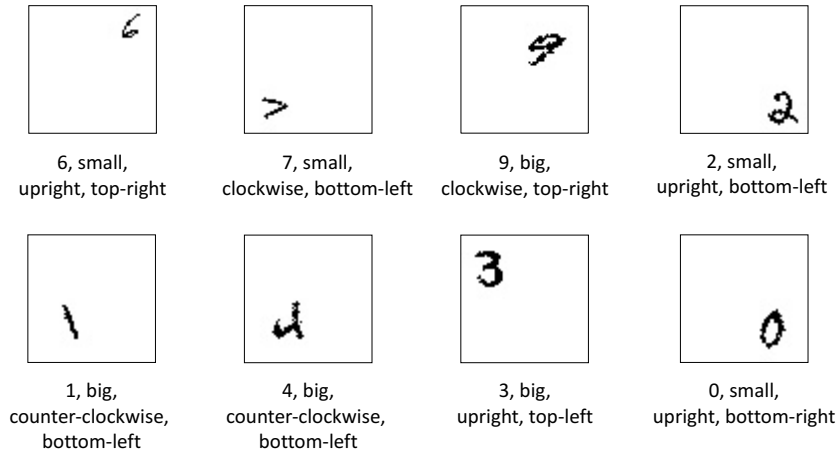


Figure 11: Example binary images from our MNIST-a dataset.

## 7.2 Details of the architectures of the encoders and decoders for the MNIST-a tasks.

As explained in the main paper, we fit the joint graphical model  $p(x, y, z) = p(z)p(x|z)p(y|z)$  with inference networks  $q(z|x, y)$ ,  $q(z|x)$ , and  $q(z|y)$ . Thus, our overall model is made up of three encoders (denoted with  $q$ ) and two decoders (denoted with  $p$ ). Across all models we use the exponential linear unit (ELU) (Clevert et al., 2015), which is a leaky non-linearity often used to train VAEs (Kingma et al., 2016). We explain the architectures in more detail below:

- **Image decoder,  $p(x|z)$ :** Our architecture for the image decoder exactly follows the standard DCGAN architecture from (Radford et al., 2015), where the input to the model is the latent state of the VAE.
- **Label decoder,  $p(y|z)$ :** Our label decoder assumes a factorized output space  $p(y|z) = \prod_{k \in \mathcal{A}} p(y_k|z)$ , where  $y_k$  is each individual attribute. We parameterize each  $p(y_k|z)$  with a two-layer MLP with 128 hidden units each. We optionally apply L1 regularization on the first layer of the MLP, which consumes as input the samples  $z$  from inference networks.

- Image and Label encoder,  $q(z|x, y)$ : Our architecture (Figure 12) for the image-label encoder first separately processes the images and the labels, and then concatenates them downstream in the network and then passes the concatenated features through a multi-layered perceptron. More specifically, we have convolutional layers which process image into 32, 64, 128, 16 feature maps with strides 1, 2, 2, 2 in the corresponding layers. We use batch normalization in the convolutional layers before applying the ELU non-linearity. On the label encoder side, we first encode the each attribute label into a 32d continuous vector and then pass each individual attribute vector through a 2-layered MLP with 512 hidden dimensions each. For example, for MNIST-a we have 4 attributes, which gives us 4 vectors of 512d. We then concatenate these vectors and pass it through a two layer MLP. Finally we concatenate this label feature with the image feature after the convolutional layers (after flattening the conv-features) and then pass the result through a 2 layer MLP to predict the mean ( $\mu$ ) and standard deviation ( $\sigma$ ) for the latent space gaussian. Following standard practice, we predict  $\log \sigma$  for the standard deviation in order to get values which are positive.

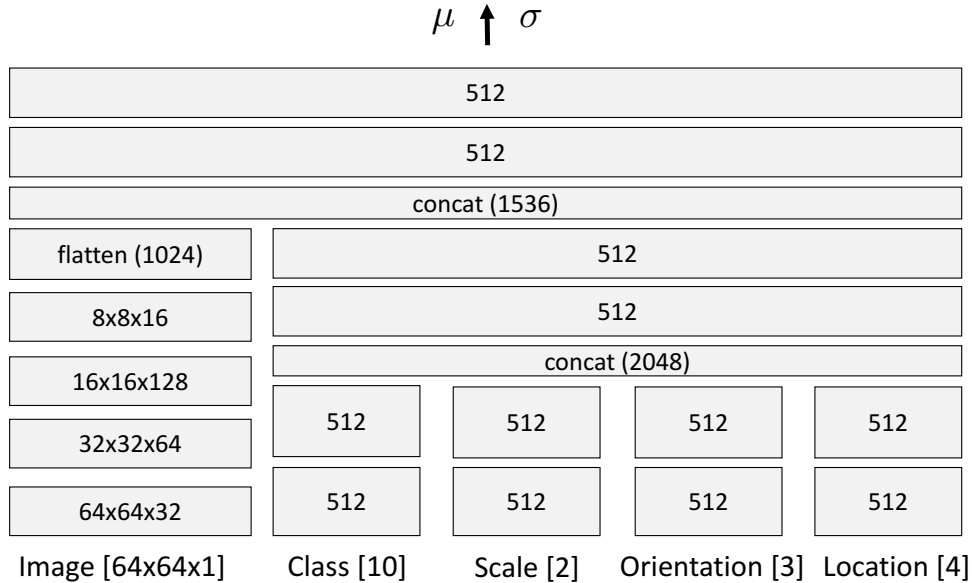


Figure 12: Architecture for the  $q(z|y)$  network in our JVAE models for MNIST-a. Images are (64x64x1), class has 10 possible values, scale has 2 possible values, orientation has 3 possible values, and location has 4 possible values.

- Image encoder,  $q(z|x)$ : The image encoder (Figure 13) uses the same architecture to process the image as the image feature extractor in  $q(z|x, y)$  network described above. After the conv-features, we pass the result through a 3-layer MLP to get the latent state mean and standard deviation vectors following the procedure described above.
- Label encoder,  $q(z|y)$ : The label encoder (Figure 14) part of the architecture uses the same design choices to process the labels as the label encoder part in the  $q(z|x, y)$  network. After obtaining the concatenated label feature vectors, we pass the result through a 4-layered MLP with 512 hidden dimensions each and then finally obtain the mean ( $\mu$ ) and  $\log \sigma$  values for each dimension in the latent state of the VAE.

### 7.3 Details on the hyperparameters for MNIST-a results.

For each method, we fix  $\lambda_x^{xy} = 1$ , but choose  $\lambda_y^{yx}$  from the range 1, 10, 50. We also use  $\ell_1$  regularization, which we sweep in the range (0, 5e-3, 5e-4, 5e-5, 5e-6, 5e-7). In addition, each way of training the model has its own method-specific hyperparameters: for JMVAE, we choose  $\alpha \in \{0.01, 0.1, 1.0\}$  (the same set of values used in (Suzuki et al., 2017)); for bi-VCCA, we choose  $\mu \in \{0.3, 0.5, 0.7\}$ ; for triple ELBO, we choose  $\lambda_y^y \in \{1, 50, 100\}$  (we keep  $\lambda_x^x = \lambda_x^{xy} = 1$ ). Thus all methods have the same number of hyperparameters.

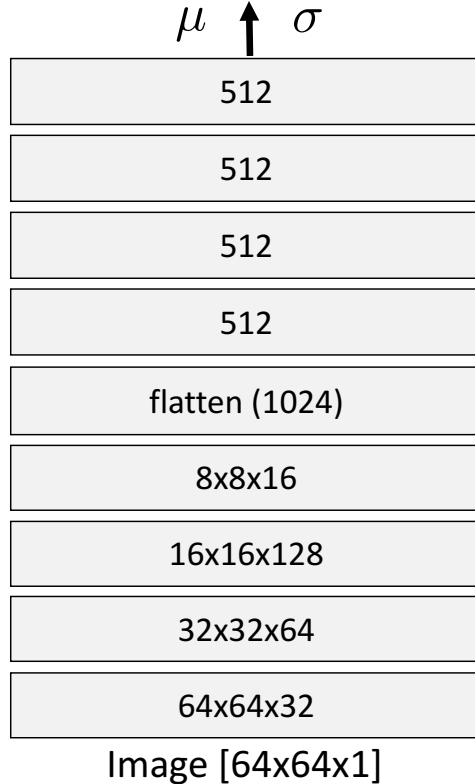


Figure 13: Architecture for the  $q(z|x)$  network in our JVAE models for MNIST-a. Images are (64x64x1) and are passed through 4 conv layers, and then through a 4-layered MLP.

We choose the best hyperparameters based on performance on the corresponding validation set. More precisely, when evaluating concrete test concepts, we choose the values that maximize the correctness score on concrete validation concepts. But when evaluating abstract test concepts, we choose the values that maximize the coverage scores on the abstract validation set. If there are multiple values with very similar coverage scores (within one standard error), we break ties by picking the values which give better correctness. The resulting hyperparameters are shown in Table 3.

#### 7.4 Details of the architectures of the encoders and decoders for the MNIST-2bit tasks.

The MNIST-2bit networks have the same general structure as described for MNIST-a, but they consist only of one-layer MLPs with ReLU activations.

- $p(x|z)$  and  $p(y|z)$ : MLPs mapping from the 2D latent space to Bernoullis of the appropriate size (784 for  $x$  and 2 for  $y$ ).
- $q(z|x, y)$ : Two MLPs, one for  $x$  and one for  $y$ . Their outputs are concatenated and then fed into another MLP. That MLP outputs 4 values, which are interpreted as  $\mu$  and  $\sigma$  for the Gaussians in the two-dimensional latent space.
- $q(z|x)$  and  $q(z|y)$ : For non-Product of Experts models, both networks are MLPs that output 4 values for the latent densities as above. If  $q(z|y)$  is a Product of Experts model, each dimension of  $y$  gets an MLP as above that takes a single bit as input.

## References

- Agrawal, A., A. Kembhavi, D. Batra, and D. Parikh (2017). C-VQA: A Compositional Split of the Visual Question Answering (VQA) v1.0 Dataset. *ArXiv*.
- Athiwaratkun, B. and A. G. Wilson (2017). Multimodal word distributions. In *Proc. ACL*.

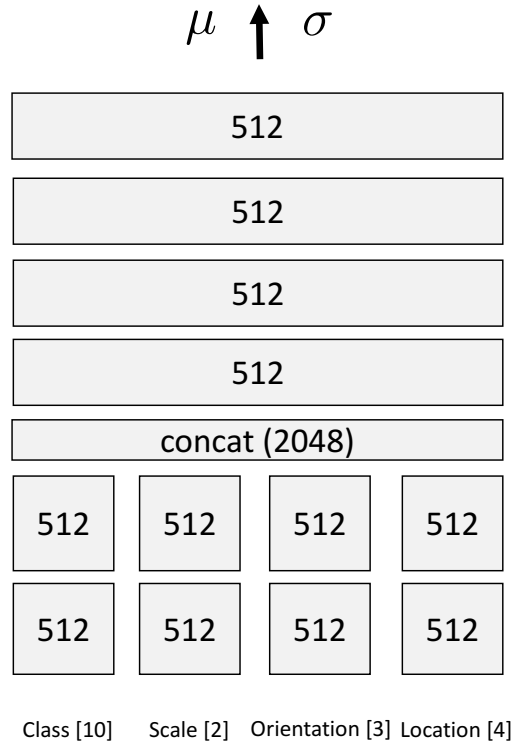


Figure 14: Architecture for the  $q(z|y)$  network in our JVAE models for MNIST-a. Class has 10 possible values, scale has 2 possible values, orientation has 3 possible values, and location has 4 possible values.

Atzmon, Y., J. Berant, V. Kezami, A. Globerson, and G. Chechik (2016, 27 August). Learning to generalize to new compositions in image understanding. *Arxiv*.

Aytar, Y., L. Castrejon, C. Vondrick, H. Pirsiavash, and A. Torralba (2016, 27 October). Cross-Modal scene networks.

Baroni, M. (2016, 1 January). Grounding distributional semantics in the visual world. *Language and Linguistics Compass* 10(1), 3–13.

Bengio, Y., L. Yao, G. Alain, and P. Vincent (2013). Generalized denoising auto-encoders as generative models. In *Advances in Neural Information Processing Systems*, pp. 899–907.

Chao, W.-L., S. Changpinyo, B. Gong, and F. Sha (2016). An empirical study and analysis of generalized Zero-Shot learning for object recognition in the wild. In *ECCV*.

Chen, X., Y. Duan, R. Houthoofd, J. Schulman, I. Sutskever, and P. Abbeel (2016). InfoGAN: Interpretable representation learning by information maximizing generative adversarial nets. In *NIPS*.

Chen, X., D. P. Kingma, T. Salimans, Y. Duan, P. Dhariwal, J. Schulman, I. Sutskever, and P. Abbeel (2017). Variational lossy autoencoder. In *ICLR*.

Chen, X. and C. L. Zitnick (2015). Mind’s eye: A recurrent visual representation for image caption generation. In *CVPR*.

Chomsky, N. (1965). *Aspects of the Theory of Syntax*. MIT Press.

Clevert, D.-A., T. Unterthiner, and S. Hochreiter (2015). Fast and accurate deep network learning by exponential linear units (elus). In *ICLR*.

de Sa, V. and D. Ballard (1998, 1 July). Category learning through multimodality sensing. *Neural Comput.* 10(5), 1097–1117.

Denton, E. and V. Birodkar (2017, 31 May). Unsupervised learning of disentangled representations from video.

Table 3: Here we list the hyperparameters used by each method to produce the results in Table 2. (Recall that we fix  $\lambda_x^{xy} = 1$  for all methods, and  $\lambda_x^x = \lambda_x^{xy}$  for triple ELBO.)

Method	#Attributes	$\lambda_y^{yx}$	Private Hyperparameter	L1	POE?	Training set
triple ELBO	4	10	$\lambda_y^y = 100$	5e-05	N	iid
JMVAE	4	50	$\alpha = 1$	0	N	iid
bi-VCCA	4	10	$\mu = 0.7$	5e-07	N	iid
triple ELBO	3	50	$\lambda_y^y = 1$	5e-03	Y	iid
JMVAE	3	50	$\alpha = 1$	5e-03	Y	iid
bi-VCCA	3	50	$\mu = 0.7$	5e-04	Y	iid
triple ELBO	2	50	$\lambda_y^y = 1$	5e-03	Y	iid
JMVAE	2	50	$\alpha = 1$	5e-03	Y	iid
bi-VCCA	2	50	$\mu = 0.7$	5e-04	Y	iid
triple ELBO	1	50	$\lambda_y^y = 1$	5e-3	Y	iid
JMVAE	1	50	$\alpha = 1$	5e-06	Y	iid
bi-VCCA	1	50	$\mu = 0.7$	5e-04	Y	iid
triple ELBO	4	10	$\lambda_y^y = 100$	0	Y	comp
JMVAE	4	50	$\alpha = 1$	5e-03	Y	comp
bi-VCCA	4	10	$\mu = 0.7$	5e-05	Y	comp

Dietterich, T. G. and G. Bakiri (1995). Solving multiclass learning problems via ECOCs. *J. of AI Research* 2, 263–286.

G. A. Miller, R. Beckwith, C. D. F. D. G. K. M. (1990). Wordnet: An online lexical database. *Int. J. Lexicography* 3(4), 235–244.

Goodfellow, I. J., J. Pouget-Abadie, M. Mirza, B. Xu, D. Warde-Farley, S. Ozair, A. Courville, and Y. Bengio (2014). Generative adversarial networks. In *NIPS*.

Harnard, S. (1990). The symbol grounding problem. *Physica D* 42, 335–346.

Higgins, I., L. Matthey, A. Pal, C. Burgess, X. Glorot, M. Botvinick, S. Mohamed, and A. Lerchner (2017). beta-VAE: Learning basic visual concepts with a constrained variational framework. In *ICLR*.

Higgins, I., N. Sonnerat, L. Matthey, A. Pal, C. P. Burgess, M. Botvinick, D. Hassabis, and A. Lerchner (2017, 11 July). SCAN: Learning abstract hierarchical compositional visual concepts.

Hinton, G. E. (2002, August). Training products of experts by minimizing contrastive divergence. *Neural Comput.* 14(8), 1771–1800.

Johnson, J., B. Hariharan, L. van der Maaten, L. Fei-Fei, C. Lawrence Zitnick, and R. Girshick (2017). CLEVR: A diagnostic dataset for compositional language and elementary visual reasoning. In *CVPR*.

Kingma, D. and J. Ba (2015). Adam: A method for stochastic optimization. In *ICLR*.

Kingma, D. P., D. J. Rezende, S. Mohamed, and M. Welling (2014). Semi-Supervised learning with deep generative models. In *NIPS*.

Kingma, D. P., T. Salimans, and M. Welling (2016). Improving variational inference with inverse autoregressive flow. In *NIPS*.

Kingma, D. P. and M. Welling (2014). Auto-encoding variational Bayes. In *ICLR*.

Lampert, C. H., H. Nickisch, and S. Harmeling (2013). Attribute-based classification for zero-shot visual object categorization. *IEEE PAMI* 36(3).

Lin, X. and D. Parikh (2015). Don’t just listen, use your imagination: Leveraging visual common sense for non-visual tasks. In *CVPR*.

Maji, S. (2017). A taxonomy of part and attribute discovery techniques. In R. S. Feris, C. Lampert, and D. Parikh (Eds.), *Visual Attributes*, Advances in Computer Vision and Pattern Recognition, pp. 247–268. Springer International Publishing.

- Mansimov, E., E. Parisotto, L. J. Ba, and R. Salakhutdinov (2016). Generating images from captions with attention.
- Mathieu, M. F., J. J. Zhao, J. Zhao, A. Ramesh, P. Sprechmann, and Y. LeCun (2016). Disentangling factors of variation in deep representation using adversarial training. In *NIPS*.
- Misra, I., A. Gupta, and M. Hebert (2017). From red wine to red tomato: Composition with context. In *CVPR*.
- Mukherjee, T. and T. Hospedales (2016). Gaussian visual-linguistic embedding for zero-shot recognition. In *Proc. Empirical Methods in Natural Language Processing*.
- Pandey, G. and A. Dukkipati (2017). Variational methods for conditional multimodal deep learning. In *Intl. J. Conf. on Neural Networks*.
- Piech, C., J. Spencer, J. Huang, S. Ganguli, M. Sahami, L. Guibas, and J. Sohl-Dickstein (2015). Deep knowledge tracing. In *NIPS*.
- Pu, Y., Z. Gan, R. Heno, X. Yuan, C. Li, A. Stevens, and L. Carin (2016). Variational autoencoder for deep learning of images, labels and captions. In *NIPS*, pp. 2352–2360.
- Radford, A., L. Metz, and S. Chintala (2015, 19 November). Unsupervised representation learning with deep convolutional generative adversarial networks. *arXiv [cs.LG]*.
- Reed, S., Z. Akata, X. Yan, L. Logeswaran, B. Schiele, and H. Lee (2016). Generative adversarial text-to-image synthesis. In *ICML*.
- Ren, Z., H. Jin, Z. Lin, C. Fang, and A. Yuille (2016, 1 October). Joint Image-Text representation by gaussian Visual-Semantic embedding. In *Proc. ACM conf. on Multimedia*, pp. 207–211. ACM.
- Russakovsky, O., J. Deng, H. Su, J. Krause, S. Satheesh, S. Ma, Z. Huang, A. Karpathy, A. Khosla, M. Bernstein, A. C. Berg, and L. Fei-Fei (2015, April). ImageNet Large Scale Visual Recognition Challenge. *International Journal of Computer Vision (IJCV)*, 1–42.
- Salakhutdinov, R. and I. Murray (2008). On the quantitative analysis of deep belief networks. In *ICML*, New York, NY, USA. ACM.
- Scarf, D., H. Hayne, and M. Colombo (2011, 23 December). Pigeons on par with primates in numerical competence. *Science* 334(6063), 1664.
- Soatto, S. and A. Chiuro (2016). Visual representations: Defining properties and deep approximations. In *ICLR*.
- Sohn, K., H. Lee, and X. Yan (2015). Learning structured output representation using deep conditional generative models. In *NIPS*.
- Suzuki, M., K. Nakayama, and Y. Matsuo (2017). Joint multimodal learning with deep generative models. In *ICLR Workshop*.
- Tenenbaum, J. B. (1999). Bayesian modeling of human concept learning. In *NIPS*.
- Theis, L., A. van den Oord, and M. Bethge (2016). A note on the evaluation of generative models. In *ICLR*.
- Vendrov, I., R. Kiros, S. Fidler, and R. Urtasun (2016). Order-Embeddings of images and language. In *ICLR*.
- Vilnis, L. and A. McCallum (2015). Word representations via gaussian embedding. In *ICLR*.
- Wang, W., H. Lee, and K. Livescu (2016, 11 October). Deep variational canonical correlation analysis. *arXiv [cs.LG]*.
- White, T. (2016). Sampling generative networks.
- Xian, Y., B. Schiele, and Z. Akata (2017). Zero-Shot learning - the good, the bad and the ugly. In *CVPR*.
- Yan, X., J. Yang, K. Sohn, and H. Lee (2016). Attribute2Image: Conditional image generation from visual attributes. In *ECCV*.
- Young, P., A. Lai, M. Hodosh, and J. Hockenmaier (2014, Feb). From image descriptions to visual denotations: New similarity metrics for semantic inference over event descriptions. *Trans. Assoc. Comp. Ling.*, 67–78.